© 2021. Published by The Company of Biologists Ltd | Journal of Cell Science (2021) 134, jcs258875. doi:10.1242/jcs.258875

RESEARCH ARTICLE

CREB regulates the expression of type 1 inositol 1,4,5-trisphosphate receptors

Vikas Arige, Lara E. Terry, Sundeep Malik, Taylor R. Knebel, Larry E. Wagner II and David I. Yule*

ABSTRACT

Inositol 1,4,5-trisphosphate (IP_3) receptors (IP_3Rs) play a central role in regulating intracellular Ca^{2+} signals in response to a variety of internal and external cues. Dysregulation of IP_3R signaling is the underlying cause for numerous pathological conditions. It is well established that the activities of IP_3Rs are governed by several post-translational modifications, including phosphorylation by protein kinase A (PKA). However, the long-term effects of PKA activation on expression of IP_3R subtypes remains largely unexplored. In this report, we investigate the effects of chronic stimulation and tonic activity of PKA on the expression of IP_3R subtypes. We demonstrate that expression of the type 1 IP_3R (IP_3R1) is augmented upon prolonged activation of PKA or upon ectopic overexpression of cyclic AMP-response element-binding protein (CREB) without altering IP_3R2 and IP_3R3 abundance. By contrast, inhibition of PKA or blocking CREB diminished IP_3R1 expression. We also demonstrate that agonist-induced Ca^{2+}-release mediated by IP_3R1 is significantly attenuated upon blocking of CREB. Moreover, CREB – by regulating the expression of KRAS-induced actin-interacting protein (KRAP) – ensures correct localization and licensing of IP_3R1. Overall, we report a crucial role for CREB in governing both the expression and correct localization of IP_3R1.

This article has an associated First Person interview with the first author of the paper.

KEY WORDS: Ca^{2+} signaling, Ca^{2+} puffs, Cyclic AMP-response element-binding protein, CREB, Inositol 1,4,5-trisphosphate receptors, IP_3Rs, KRAS-induced actin-interacting protein, KRAP, ITPR-interacting domain containing 2, ITPRID2, Total internal reflection fluorescence microscopy, TIRF

INTRODUCTION

Inositol 1,4,5-trisphosphate (IP_3) receptor (IP_3R)-mediated redistribution of Ca^{2+} from the endoplasmic reticulum to the cytosol and other organelles occurs upon binding of IP_3 (and the co-agonist Ca^{2+}). IP_3 is formed in response to a number of hormones, growth factors or neurotransmitters that activate phospholipase C isoforms (Berridge et al., 2000; Bootman et al., 2002; Clapham, 2007). The subsequent increase in intracellular Ca^{2+} regulates a myriad of physiological processes including secretion, contraction, gene transcription, proliferation, apoptosis, oxidative phosphorylation, learning and memory (Berridge et al., 2000; Clapham, 2007; Decuypere et al., 2011; Foskett et al., 2007). Humans have three types of IP_3Rs: type 1 (IP_3R1), type 2 (IP_3R2) and type 3 (IP_3R3), which are encoded by *ITPR1*, *ITPR2* and *ITPR3*, respectively (Berridge, 1993; Bezprozvanny, 2005; Blondel et al., 1993; Furuichi et al., 1989; Südhof et al., 1991). Each isoform has a molecular mass of ∼300 kDa, they share 60-70% sequence similarity, and are assembled as homo- and hetero-tetrameric Ca^{2+} channels that predominantly localize to the endoplasmic reticulum (Mignery et al., 1989; Monkawa et al., 1995; Wojcikiewicz and He, 1995). IP_3R subtypes differ in their binding affinities for IP_3 (Iwai et al., 2007; Newton et al., 1994). Their activity is differentially modulated by various post-translational modifications, including phosphorylation by protein kinase A (PKA) (Masuda et al., 2010), PKC, CaMKII (Ferris et al., 1991b), AKT (Khan et al., 2006), ubiquitylation (Alzayady and Wojcikiewicz, 2005), glycosylation (Rengifo et al., 2007), redox state of cells (Joseph et al., 2018), binding to ATP (Bezprozvanny and Ehrlich, 1993) and interaction with other proteins (Prole and Taylor, 2016).

IP_3Rs are ubiquitously expressed; however, their expression is regulated in a tissue- and development-specific manner (De Smedt et al., 1997; Newton et al., 1994). For example, IP_3R1 is predominantly expressed in the central nervous system while IP_3R2 and IP_3R3 are enriched in the peripheral tissues (Alzayady et al., 2013; Furuichi et al., 1989; Wojcikiewicz, 1995). IP_3R1 knockout mice predominately die *in utero* or very early during post-natal development as a result of severe ataxia and seizures (Matsumoto et al., 1996; van de Leemput et al., 2007). Individual IP_3R2 or IP_3R3 knockout mice, by contrast, develop normally with subtle phenotypes; however, the dual IP_3R2–IP_3R3 knockout animal displays severe defects in salivary, pancreatic and lacrimal exocrine secretion, and die shortly after weaning due to their inability to assimilate macronutrients (Futatsugi et al., 2005). Moreover, perturbations in IP_3R signaling or mutations in IP_3Rs (Foskett, 2010; Terry et al., 2020) are associated with several pathological conditions, including Alzheimer disease (Cheung et al., 2010), Huntington disease (Tang et al., 2005), schizophrenia (Tsuboi et al., 2015), amyotrophic lateral sclerosis (van Es et al., 2007), spinocerebellar ataxia (Ando et al., 2018; Ogura et al., 2001), Gillespie syndrome (Gerber et al., 2016), anhidrosis (Klar et al., 2014), diabetes (Roach et al., 2006) and cancer (Ueasilamongkol et al., 2020).

Previous reports also indicate that the number of IP_3Rs can be acutely regulated. For example, Ca^{2+} influx through the L-type Ca^{2+}-channels or NMDA receptors augments expression of IP_3R1 in neuronal cultures (Genazzani et al., 1999; Graef et al., 1999). Similarly, the heteromeric transcription factor activator protein 1 (AP-1) and nuclear factor of activated T-cells 4 (NFATc4) augments IP_3R1 expression in mouse cerebral cortical neurons (Mizuno et al., 2012, 2015). The box-I, which is located at position −334 to −318 bp

Department of Pharmacology and Physiology, University of Rochester, Rochester, NY 14642, USA.

*Author for correspondence (david_yule@urmc.rochester.edu)

V.A., 0000-0002-0589-1880; L.E.T., 0000-0002-0200-4334; D.I.Y., 0000-0002-6743-0668

Handling Editor: John Heath
Received 5 May 2021; Accepted 13 September 2021

Journal of Cell Science (2021) 134, jcs258875. doi:10.1242/jcs.258875

relative to the transcription initiation site, in the *cis*-promoter region of *Itpr1* was shown to be required for expression of IP_3R1 in mouse neural crest-derived neuroblastoma (N2a) cells (Konishi et al., 1997). Moreover, 12-O-tetradecanoylphorbol-13-acetate (TPA) or serum were shown to activate, whereas 1,25-dihydroxyvitamin D3 or 17β-estradiol were shown to inhibit *ITPR1* promoter activity (Kirkwood et al., 1997). Likewise, TGF-β is known to increase the phosphorylation of IP_3R1 while inhibiting its expression in mesangial cells (Sharma et al., 1997). TGF-β is also known to inhibit the expression of IP_3R1 and IP_3R3 in pre-glomerular afferent arteriolar smooth muscle cells (Pacher et al., 2008). We have previously reported that TNF-α augments the activity and expression of IP_3R1 via the transcription factor SP1 (Park et al., 2008, 2009). Nuclear factor erythroid 2-related factor 2 (NFE2L2) inhibits the expression of IP_3R3 in both rat and human cholangiocytes by binding to musculo-aponeurotic fibrosarcoma recognition element (MARE) in the *ITPR3* promoter (Weerachayaphorn et al., 2015). At the post-transcriptional level, microRNAs miR-133a and miR-506 inhibit the expression of IP_3R2 and IP_3R3, respectively (Ananthanarayanan et al., 2015; Drawnel et al., 2012). The expression of IP_3Rs is also induced by exposure to methamphetamine or cocaine (Kurokawa et al., 2012). However, additional molecular factors regulating the expression of IP_3Rs have so far remained largely underexplored.

Although several reports have clearly established the short-term/acute effects of raising intracellular levels of cAMP upon both the activity and phosphorylation status of IP_3Rs (Ferris et al., 1991a; Patel et al., 1999; Soulsby and Wojcikiewicz, 2005; Wagner et al., 2008, 2004, 2003), any long-term consequences of PKA activity have not been defined. In our present study, we examined the long-term effects of chronic stimulation of PKA on the expression of IP_3Rs in HEK-293 cells. Our results indicate that the endogenous protein levels of IP_3R1 are augmented in response to increasing PKA activity by exposure to forskolin, whereas the protein levels of IP_3R2 and IP_3R3 remain unaffected. We also show that this effect is mediated through the transcription factor cyclic AMP-response element-binding protein (CREB). Consistent with this observation, ectopic overexpression of constitutively active CREB in HEK-293 cells augmented protein levels of IP_3R1 and ITPR-interacting domain containing 2 (ITPRID2, also known as and hereafter referred to as KRAP), a binding partner of IP_3R that is important for agonist-induced Ca^{2+} release, localization and function (Fujimoto et al., 2011b; Thillaiappan et al., 2021). This transcriptional regulation of IP_3R1 levels had functional consequences, as dominant-negative CREB transfection significantly diminished agonist-induced Ca^{2+} release and, notably, 'Ca^{2+} puffs' – the elementary Ca^{2+} signals generated by IP_3Rs. Overexpression of VP16-CREB – a constitutively active form of CREB – increased the Ca^{2+} puff activity. Taken together, our results indicate a crucial role for CREB in governing the expression of *ITPR1* through its endogenous promoter and, subsequently, the underlying agonist-evoked Ca^{2+} puffs by IP_3R1 in HEK-293 cells.

RESULTS

Previous results from our laboratory and other groups have conclusively documented that all the three IP_3Rs are phosphorylated by PKA (Wagner et al., 2008; Wojcikiewicz and Luo, 1998). The sites of phosphorylation and the acute functional consequences of phosphorylation regarding IP_3R activity have also been extensively studied (Soulsby et al., 2004). Nevertheless, the long-term effects of PKA activation on the endogenous protein levels of IP_3Rs, i.e. the stimulus–transcriptional coupling, have not been fully determined.

Forskolin augments protein expression of IP_3R1 in HEK-293 cells

To investigate whether PKA activation has any long-term effects on the endogenous protein levels of IP_3Rs, we treated HEK-293 cells with 10 µM forskolin for 12 h to raise intracellular cAMP and activate PKA, and then determined IP_3R protein levels by western blotting. We found that the endogenous protein levels of IP_3R1 significantly increased following treatment with 10 µM forskolin (Fig. 1A,B) but that the endogenous protein levels of IP_3R2 (Fig. 1C,D) and IP_3R3 (Fig. 1E,F) remained unaltered. Moreover, treatment with 10 µM forskolin augmented endogenous IP_3R1 protein levels in a time-dependent manner (Fig. S1). Consistently, the IP_3R1 remained phosphorylated following 12 h treatment with 10 µM forskolin (Fig. S2). These results indicated that long-term treatment with forskolin augments both endogenous levels of IP_3R1 protein and the extent to which the receptor remains phosphorylated in HEK-293 cells.

In silico analysis reveals putative binding sites for CREB in the proximal promoter domains of IP_3Rs

Forskolin activates adenylyl cyclase, resulting in increased levels of intracellular cAMP (Insel and Ostrom, 2003). cAMP binds to the regulatory subunits of PKA, with the important consequence that free catalytic subunits translocate into the nucleus, where they phosphorylate and activate the transcription factor CREB. Once phosphorylated, CREB recruits the transcriptional machinery required for the transcription of target genes (Altarejos and Montminy, 2011). Since forskolin treatment augmented the endogenous protein level of IP_3R1, we employed several *in silico* transcription factor-binding prediction tools, including Alibaba2.1, TFBIND, Consite and PROMO, which all rely on different algorithms to predict CREB-binding sites within the 1 kb proximal promoter domains of IP_3Rs. Interestingly, three out of four tools predicted at least one CREB-binding site within the proximal promoter domain of all the three IP_3Rs (Fig. 2A). In addition, these tools also predicted binding sites for other transcription factors, such as SP1, EGR1 and NF-KB amongst others. This concurs with a previous report by our group wherein we demonstrated that SP1 is involved in regulating the gene expression and protein synthesis of IP_3R1 (Park et al., 2009). To functionally validate our *in silico* predictions, we performed luciferase assays using reporter constructs comprising the *ITPR1* or *ITPR2* promoter. Co-transfection of the 1 kb proximal *ITPR1* promoter-reporter construct with VP16-CREB expression plasmid resulted in a dose-dependent increase in promoter activity (Fig. 2B). VP16-CREB binds the cAMP response element (CRE) through the DNA-binding domain of CREB and transcriptional activation is facilitated by transcriptional activation domain of the herpes virus VP16 protein (Riccio et al., 1999). In contrast, the *ITPR1* promoter activity diminished upon co-transfection with a dominant-negative form of CREB (i.e. KCREB) (Fig. 2C) or upon treatment with 20 µM of the PKA inhibitor H89 (Fig. 2D). KCREB plasmid, encoding a dominant-negative form of CREB, was transfected into HEK-293 cells to block endogenous CREB (Walton et al., 1992). The reduction in *ITPR1* promoter activity following co-transfection of KCREB or exposure to H89 suggested that activation of PKA under basal conditions plays an important role in regulating the transcription of *ITPR1* in these cells, which is consistent with the observation that basal PKA activity is relatively high in HEK-293 cells (Mignen et al., 2005). A similar increase in the promoter activity was observed when the *ITPR2* promoter-reporter construct was co-transfected with the VP16-CREB expression plasmid

Journal of Cell Science (2021) 134, jcs258875. doi:10.1242/jcs.258875

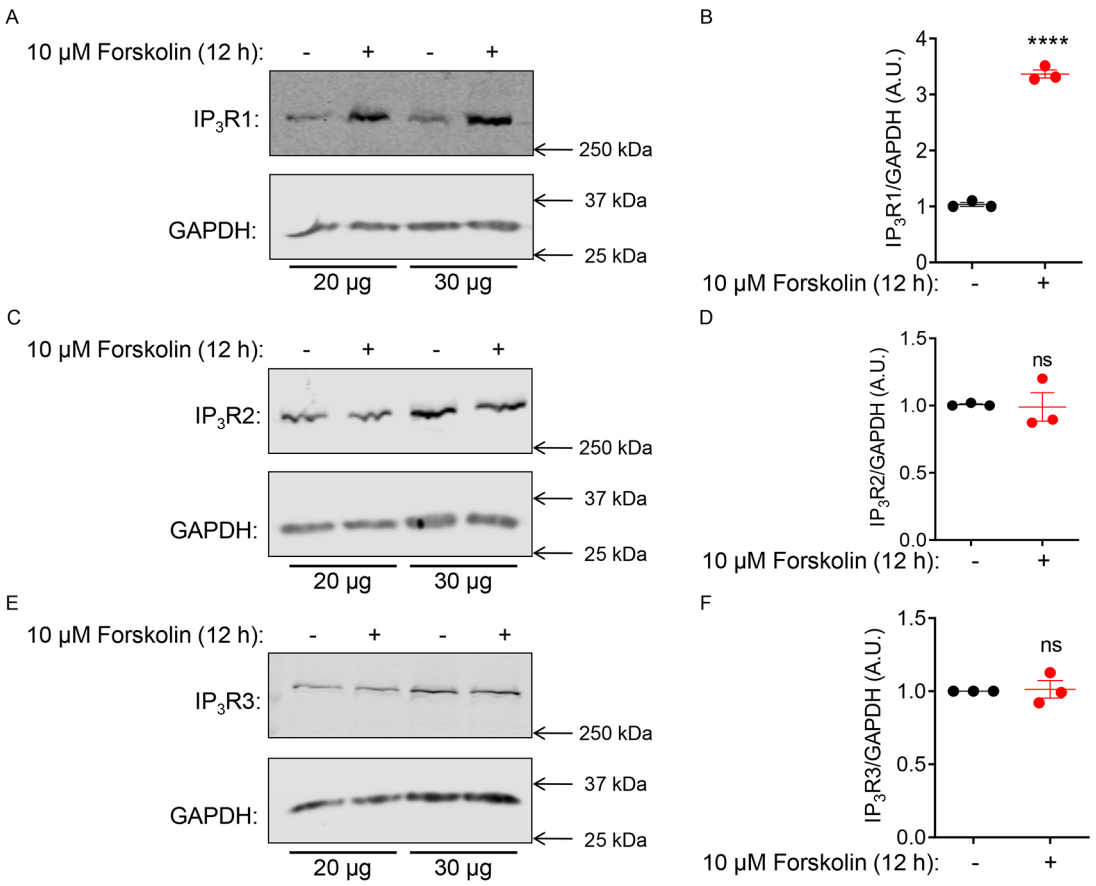

Fig. 1. Forskolin augments the endogenous protein levels of IP_3R1 in HEK-293 cells. HEK-293 cells were treated with 10 µM forskolin for 12 h followed by protein isolation. (A,C,E) Representative western blots showing forskolin-induced endogenous protein levels of IP_3R1 (A), IP_3R2 (C) and IP3R3 (E). Total amount of protein loaded: 20 µg or 30 µg as indicated. (B,D,F) Quantitative analysis of three independent western blots for experimental scenarios described under A, C and E. Statistical significance was determined by Student's *t*-test (unpaired, two-tailed). ****P<0.0001. ns, not significant.

(Fig. 2E) that previously had been shown to be regulated by CREB (Kruglov et al., 2017). These results indicate a potential role for CREB in governing expression of both *ITPR1* and *ITPR2*.

Correlation between transcript levels of genes encoding IP_3Rs and CREB across human tissues

To determine whether there is any correlation between the transcript levels of IP_3Rs and CREB, we next mined transcriptomics data for *CREB1*, *ITPR1*, *ITPR2* and *ITPR3* from GTEx database, a publicly available database. The transcript levels of *ITPR1*, *ITPR2* and *ITPR3* displayed significant positive correlations when compared with those of *CREB1* in 54 different tissue types (Fig. 2F–H; Table S1). Taken together with the predictions of *in silico* transcription factors and our *in vitro* promoter-reporter assays, these results indicate a role for CREB in regulating the expression of IP_3Rs across various human tissues.

Involvement of the PKA–CREB axis in regulating the expression of IP_3R1

To dissociate the acute effects of IP_3R1 phosphorylation and to demonstrate the involvement of CREB in regulating the expression of IP_3Rs, increasing amounts of the constitutively active VP16-CREB-expression plasmid was transfected into HEK-293 cells followed by western blotting to determine the endogenous protein levels of the three IP_3Rs subtypes. Interestingly, transient transfection of constitutively active VP16-CREB augmented the endogenous protein levels of IP_3R1 (Fig. 3A,B), whereas levels of IP_3R2 and IP_3R3 remained unaltered (Fig. S3A,B). To substantiate the role of CREB regarding the levels of IP_3R1, the dominant-negative KCREB plasmid was transfected into HEK-293 cells to inhibit endogenous CREB. In this case, western blotting revealed that KCREB transfection resulted in a concentration-dependent decrease in the endogenous IP_3R1 protein levels within HEK-293 cells (Fig. 3C,D). These results indicated that, under basal conditions, CREB regulates the levels of IP_3R1 protein and that IP_3R1 is a bona fide target of CREB in HEK-293 cells.

Since treatment of cells with forskolin activates PKA, we assessed the role PKA has in regulating the expression of IP_3R1 through CREB. For this, a PKA inhibitor (PKI) plasmid (Day et al., 1989) was transiently transfected into HEK-293 cells followed by western blotting to probe for endogenous IP_3R1 levels. As expected, transfection of the PKI plasmid resulted in a decrease in endogenous IP_3R1 protein levels within HEK-293 cells (Fig. 3E,F), which further emphasizes a role of PKA in regulating IP_3R1 under basal conditions. Our results indicate that the PKA–CREB axis is involved in regulating the expression of IP_3R1 in HEK-293 cells.

Does PKA also play a similar role in regulating the expression of IP_3R1 in other cell lines? To address this, we treated human neuroblastoma SH-SY5Y and HeLa cells with the PKA inhibitor H89 for 12 h. Compared with untreated controls, the endogenous levels of IP_3R1 protein diminished in both SH-SY5Y and HeLa cells upon treatment with H89 (Fig. S4A,C). These results indicate a role for PKA in governing IP_3R1 expression across various cell lines.

Journal of Cell Science (2021) 134, jcs258875. doi:10.1242/jcs.258875

A

Tool	Alibaba2.1		TFBIND		ConSite		PROMO	
	CREB	SP1	CREB	SP1	CREB	SP1	CREB	SP1
ITPR1	+	+	+	+	+	+	-	+
ITPR2	+	+	+	+	+	+	+	+
ITRP3	+	+	+	+	+	+	+	+

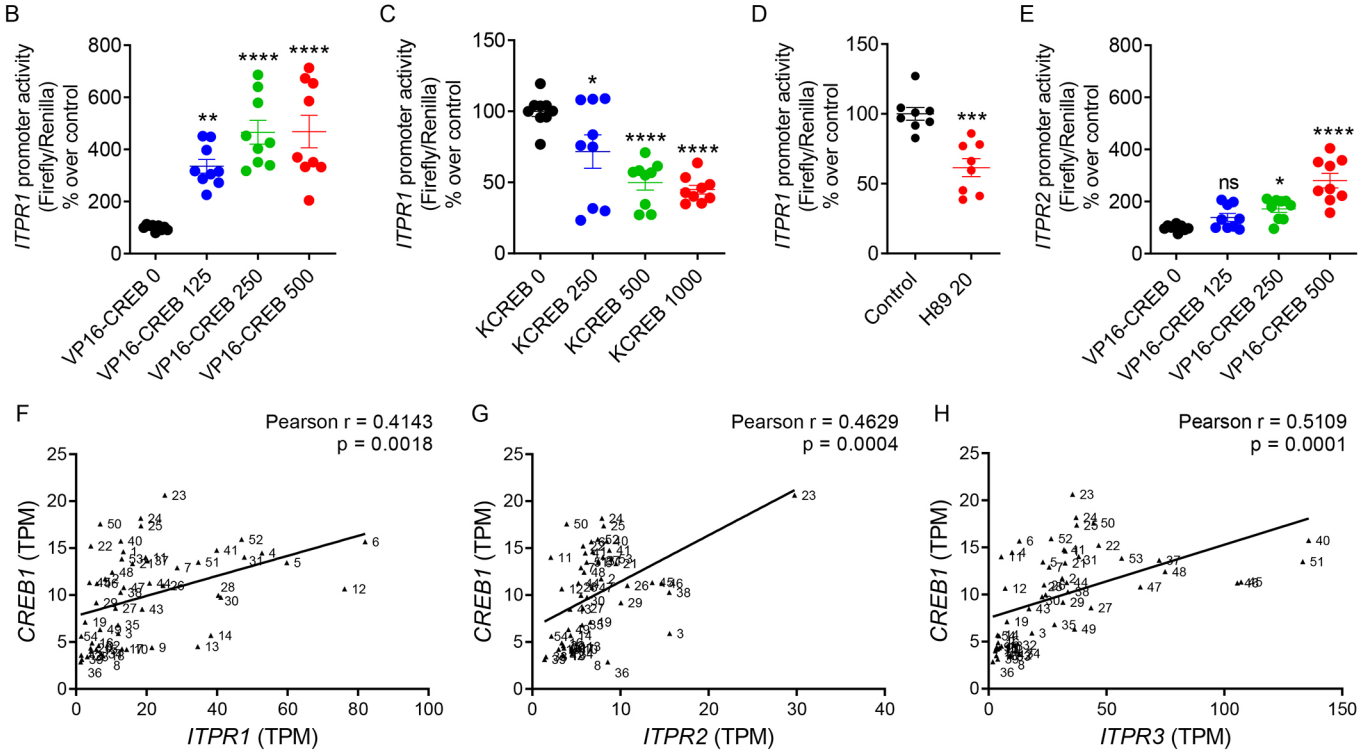

Fig. 2. *In silico* analysis revealed putative binding sites for CREB in the proximal promoter domains of *ITPR1, ITPR2* and *ITPR3*. (A) Results from the computational analysis by using various transcription factor prediction tools to predict putative binding sites for CREB and SP1 in the 1 kb proximal-promoter domains of *ITPR1*, *ITPR2* and *ITPR3*. + and – denote predicted and not predicted, respectively. (B) Co-transfection of the *ITPR1* promoter-reporter construct with no (0, black), or 125, 250 or 500 ng (blue, green or red, respectively) of VP16-CREB expression plasmid resulted in a dose-dependent increase in *ITPR1* promoter activity. (C) Co-transfection of the *ITPR1* promoter-reporter construct with no (0, black), or 250, 500 or 1000 ng (blue, green or red, respectively) of KCREB plasmid (ng) resulted in a dose-dependent decrease in *ITPR1* promoter activity. (D) *ITPR1* promoter activity decreased upon treatment with 20 µM H89 (red), compared with that upon control treatment. (E) Co-transfection of the *ITPR2* promoter-reporter construct with no (0, black), or 125, 250 or 500 ng (blue, green or red, respectively) of VP16-CREB expression plasmid resulted in a dose-dependent increase in *ITPR2* promoter activity. Statistical significance was determined by Student's *t*-test (unpaired, two-tailed) or one-way ANOVA with Tukey's multiple comparisons post-test. **P*<0.05, ***P*<0.01, ****P*<0.001, *****P*<0.0001. ns, not significant. (F–H) Plots of RNAseq data mined by using the GTEx portal display significant positive correlations of transcript levels of *ITPR1* vs *CREB* (F), *ITPR2* vs *CREB* (G) and *ITPR3* vs *CREB* (H) across *n*=54 human tissue types. TPM, transcripts per million.

Forskolin-induced IP_3R1 expression is mediated by CREB

To determine the involvement of CREB in mediating the effect of PKA activation above basal activity, HEK-293 cells were transiently transfected with either pcDNA as a control or KCREB, followed by treatment with 10 µM forskolin and western blotting analysis. Transfection of KCREB, i.e. expression of dominant-negative CREB, resulted in decreased IP_3R1 levels, whereas treatment with 10 µM forskolin enhanced levels further (Fig. 3G,H). Forskolin-induced endogenous IP_3R1 levels were modestly diminished upon blocking endogenous CREB (Fig. 3G,H). These results further highlight a role of CREB in forskolin-induced IP_3R1 expression.

Agonist-induced Ca^{2+} release is diminished upon blocking endogenous CREB in a population of cells

We next investigated the impact of CREB on agonist-induced Ca^{2+} release from HEK-293 cells that only express IP_3R1 at endogenous levels. These cells were engineered using CRISPR-Cas9 technology through deletion of *ITPR2* and *ITPR3* normally expressed in HEK-293 cells (Alzayady et al., 2016). These cells – hereafter referred to as hR1 endo cells – were utilized in all subsequent experiments to prevent any contribution of IP_3R2 and IP_3R3 to Ca^{2+} release by using a heterotetrameric population of IP_3Rs. Transfection of hR1 endo cells with either pcDNA or KCREB, and Ca^{2+} release in response to the muscarinic receptor agonist carbachol (CCh) was monitored by using a Flexstation plate-reader assay platform with microfluidics. The increase in cytosolic Ca^{2+} in response to increasing concentrations of CCh (0.1–100 µM) was then determined. Notably, following stimulation with sub-maximal concentration of CCh (10 µm), Ca^{2+} increase in KCREB-transfected cells was significantly less compared to cells transfected with pcDNA (Fig. 4A). These data demonstrated that KCREB transfection of hR1 endo cells results in decreased IP_3R1 expression, consistent with decreased release of Ca^{2+} in response to agonist stimulation.

Journal of Cell Science (2021) 134, jcs258875. doi:10.1242/jcs.258875

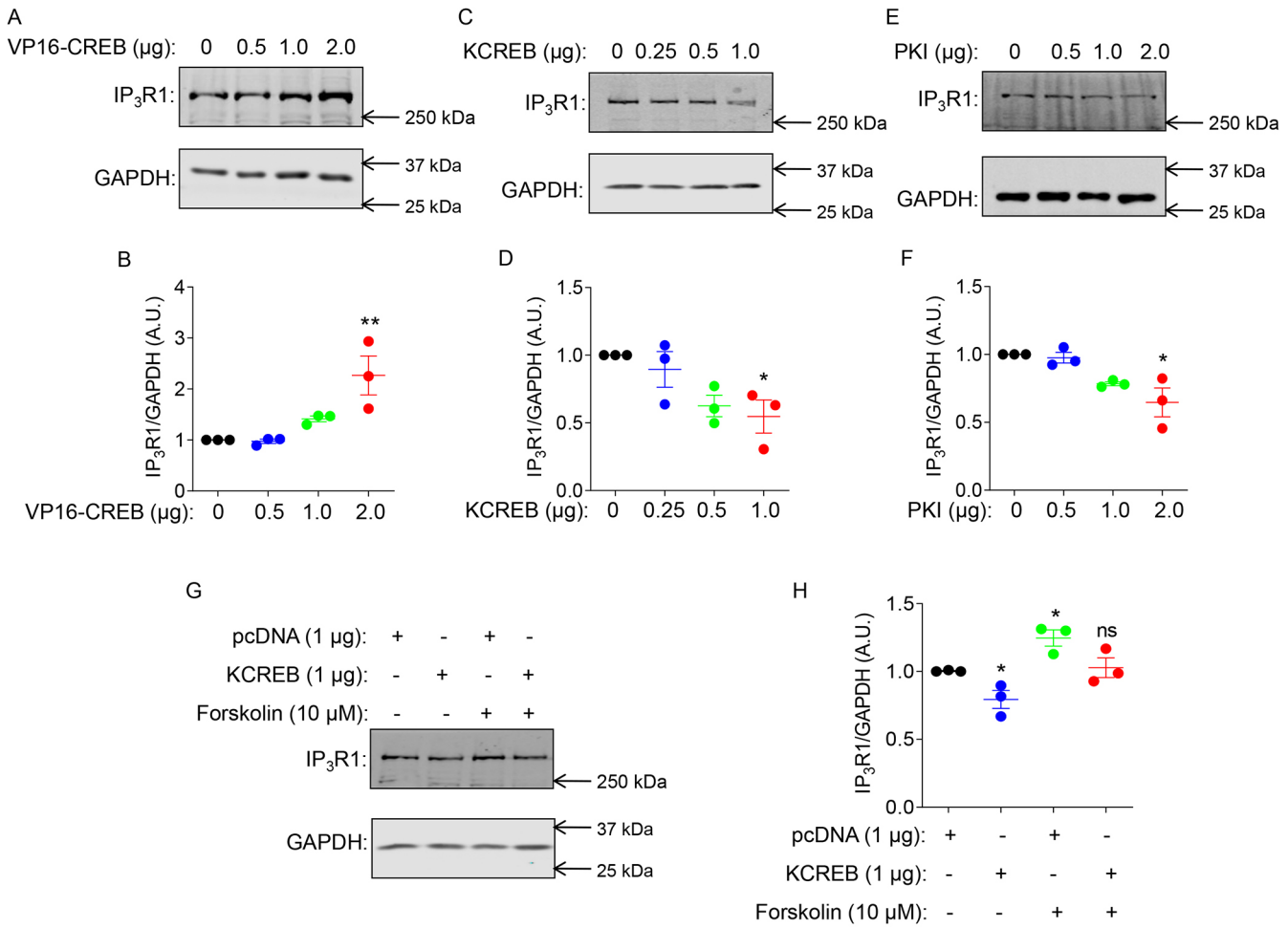

Fig. 3. Evidence for involvement of PKA–CREB axis in governing the expression of IP_3R1. (A,C,E) HEK-293 cells were not transfected (0 µg, black), or transiently transfected with 0.5, 1.0 or 2.0 µg (blue, green or red, respectively) amounts of VP16-CREB (A), KCREB (C) or PKI (E) expression plasmid; total protein amounts were isolated 36 h following transfection and analyzed by western blotting. Representative western blots are shown. Overexpression of VP16-CREB resulted in a dose-dependent increase in levels of endogenous IP_3R1 (A). Blocking endogenous CREB due to overexpression of KCREB resulted in a dose-dependent decrease of endogenous IP_3R1 (C). Inhibition of endogenous PKA due to overexpression of PKI, resulted in a dose-dependent decrease of endogenous IP_3R1 (E). (B,D,F) Quantitative analysis of three independent western blots for experimental scenarios described under A, C and E. Statistical significance was determined by one-way ANOVA with Tukey's multiple comparisons post-test. *P<0.05, **P<0.01. (G,H) HEK-293 cells were transiently transfected (+) with either pcDNA control or KCREB plasmid. After 24 h, cells were further treated with 10 µM forskolin (+) or left untreated (–) for an additional 12 h. At 36 h after transfection, protein levels were analyzed by western blotting, showing increased levels of IP_3R1 in cells treated with forskolin under basal conditions or when CREB was inhibited using KCREB, suggesting involvement of CREB in forskolin-induced expression of IP_3R1. (H) Quantitative analysis of three independent western blots for the experimental scenario described under G. Statistical significance was determined by Student's *t*-test (unpaired, two-tailed). *P<0.05 with respect to control condition. ns, not significant.

In contrast, HEK-293 cells that only express IP_3R3 – hereafter referred to as hR3 endo cells (Alzayady et al., 2016) – and were transfected with equal amounts of either pcDNA or KCREB showed no significant difference in agonist-induced Ca^{2+} release (Fig. 4B). Indeed, these results are in agreement with our observations that the endogenous protein levels of IP_3R2 and IP_3R3 remain unaltered upon overexpressing CREB (Fig. S3A,B), suggesting that the effect of CREB is specific to only the IP_3R1 subtype in HEK-293 cells.

CCh-induced Ca^{2+} release is attenuated upon blocking endogenous CREB

Given that the agonist-induced Ca^{2+} release is inhibited in a population-based assay with, presumably, non-uniform transfection efficiency, we next performed single-cell imaging using an epifluorescence microscope under which transfected cells could be optically identified. For single-cell imaging, hR1 endo cells were co-transfected with mCherry-3HA (herein referred to as mCherry) plasmid and either pcDNA or KCREB. Following 36 h of transfection, cells were loaded with 2 µM Fura-2/AM to monitor changes in cytosolic Ca^{2+} in response to increasing doses of CCh. In response to stimulation with CCh at varying concentrations, mCherry-positive hR1 endo cells transfected with KCREB displayed much lower changes in fluorescence ratio (Fig. 5B,E) compared to mCherry-positive hR1 endo cells transfected with pcDNA (Fig. 5A,D). Consistent with this, the average increases in amplitude and the peak amplitude changes tended to be lower in cells transfected with KCREB compared to those transfected with pcDNA (Fig. 5C,F,H). Moreover, the percentage of KCREB-transfected cells responding to different concentrations of CCh at a specific threshold (F/F_0>0.02, where F/F_0 represents the change of fluorescence intensity relative to basal fluorescence) were diminished when compared to pcDNA transfected cells (Fig. 6G). Overall, these results provide mechanistic insights of CREB having

Journal of Cell Science (2021) 134, jcs258875. doi:10.1242/jcs.258875

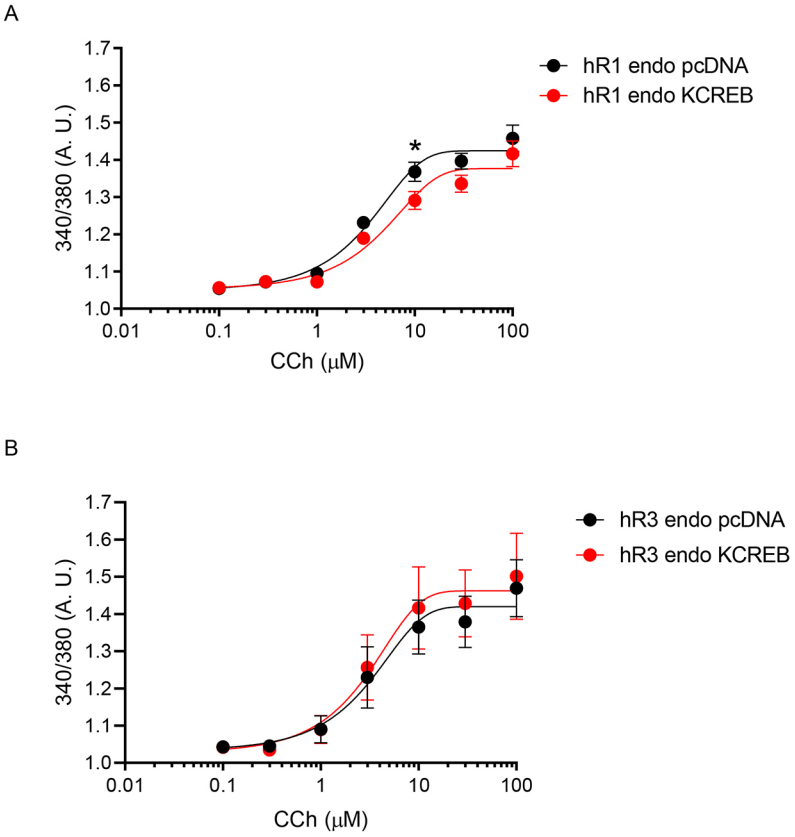

Fig. 4. Inhibition of endogenous CREB diminished agonist-induced Ca^{2+} release in a population-based Ca^{2+}-imaging assay. (A,B) $IP_3R2/3^{-/-}$ (hR1 endo) (A) or $IP_3R1/2^{-/-}$ (hR3 endo) (B) HEK-293 cells were transiently transfected with either pcDNA as control or KCREB, loaded with Fura-2/AM and imaged using a Flexstation 96-well plate reader after treatment with increasing concentrations (0.1-100 μM) of CCh. In response to treatment with ≥10 μM CCh, hR1 endo cells transfected with KCREB showed significantly diminished Ca^{2+} release compared with Ca^{2+} release in cells transfected with pcDNA (A). Identically transfected and treated hR3 endo cells, however, did not display this difference in Ca^{2+} release upon treatment with CCh. Data are presented as mean±s.e.m. Statistical significance was determined by Student's *t*-test (unpaired, two-tailed). *P<0.05.

a key role in the regulation of IP_3R1 levels and agonist-evoked Ca^{2+} release.

Diminished expression of IP_3R1 results in dampened ci-IP_3-evoked Ca^{2+} puffs

To further investigate the effect of CREB on IP_3R1 protein levels, we used total internal reflection fluorescence (TIRF) microscopy to measure elementary Ca^{2+} signals, i.e. Ca^{2+} puffs, evoked following the uncaging of a cell-permeable form of caged IP_3 (ci-IP_3) in hR1 endo cells. Paradoxically, these Ca^{2+} signals represent a small majority of IP_3R clusters that are active upon stimulation and are known as 'licensed' IP_3R (Thillaiappan et al., 2017). For this purpose, hR1 endo cells co-transfected with mCherry and pcDNA, VP16-CREB or KCREB plasmids were loaded with Cal-520 AM and caged IP_3(ci-IP_3/PM) followed by EGTA-AM, and Ca^{2+} puffs were recorded after photolysis of ci-IP_3 for 40 s at a rate of ∼97 frames per second. TIRF measurements of Ca^{2+} puffs following ci-IP_3 uncaging were designed to facilitate analysis of the fundamental properties of small IP_3R1 clusters, which are less influenced by other processes. In turn, this might influence the characteristics of the Ca^{2+} signal observed in global measurements of whole cells. Ca^{2+} puffs were detected throughout the 40 s recording period following photolysis of ci-IP_3 in hR1 endo cells co-transfected with mCherry and pcDNA, VP16-CREB or KCREB plasmids (Fig. 6A–C). We specifically imaged and analyzed only mCherry-positive cells (Movies 1, 2, and 3). Interestingly, the number of Ca^{2+}-puff sites per cell were significantly decreased in hR1 endo cells transfected with KCREB plasmid (65, n=9 cells) compared to those in cells transfected with pcDNA (281, n=9 cells) or VP16-CREB (368, n=9 cells) (Fig. 6E). Although the number of Ca^{2+}-puff sites per cell was slightly higher in cells transfected with CREB compared to those transfected with pcDNA, this increase was not statistically significant (Fig. 6E). Furthermore, similar to the number of Ca^{2+}-puff sites per cell, the number of Ca^{2+} puffs per cell remained significantly diminished in KCREB-transfected cells (109, n=9 cells) compared to those in pcDNA-transfected cells (490, n=9 cells) (Fig. 6D). In contrast, the number of Ca^{2+} puffs per cell were significantly elevated in VP16-CREB-transfected cells (1483, n=9 cells) compared to those in pcDNA-transfected cells (Fig. 6D). The amplitudes (Fig. 6F) and the mean time of a rise (r) and fall (f) in Ca^{2+}-puff fluorescence (Fig. 6G) induced by photolysis of ci-IP_3 remained similar in hR1 endo cells transfected with pcDNA, KCREB or VP16-CREB plasmid, indicating that the fundamental biophysical properties of IP_3R1 clusters remained unaltered in these cells. These data further substantiate the involvement of CREB in governing the expression of IP_3R1, which is destined to be active following agonist stimulation.

KRAP facilitates proper localization and optimizes activity of IP_3Rs, and is also a target of CREB

Based on the previous reports that KRAP is required for proper localization of IP_3Rs and in defining their ability to respond to IP_3 (Fujimoto et al., 2011a; Thillaiappan et al., 2021), we performed *in silico* analysis to investigate potential CREB binding sites within the 1 kb proximal promoter region of *ITPRID2* (encoding KRAP). Interestingly, by using various transcription factor prediction tools, our *in silico* analysis revealed putative CREB-binding sites in the proximal promoter domain of *ITPRID2* (Table S2). Furthermore, we observed an increase in endogenous protein levels of KRAP following treatment with 10 μM forskolin (Fig. 7A,B). To functionally validate the involvement of CREB in regulating *ITPRID2* expression, we transfected HEK-293 cells with VP16-CREB or KCREB plasmids followed by western blotting to determine the KRAP protein levels. Overexpression of CREB in

Journal of Cell Science (2021) 134, jcs258875. doi:10.1242/jcs.258875

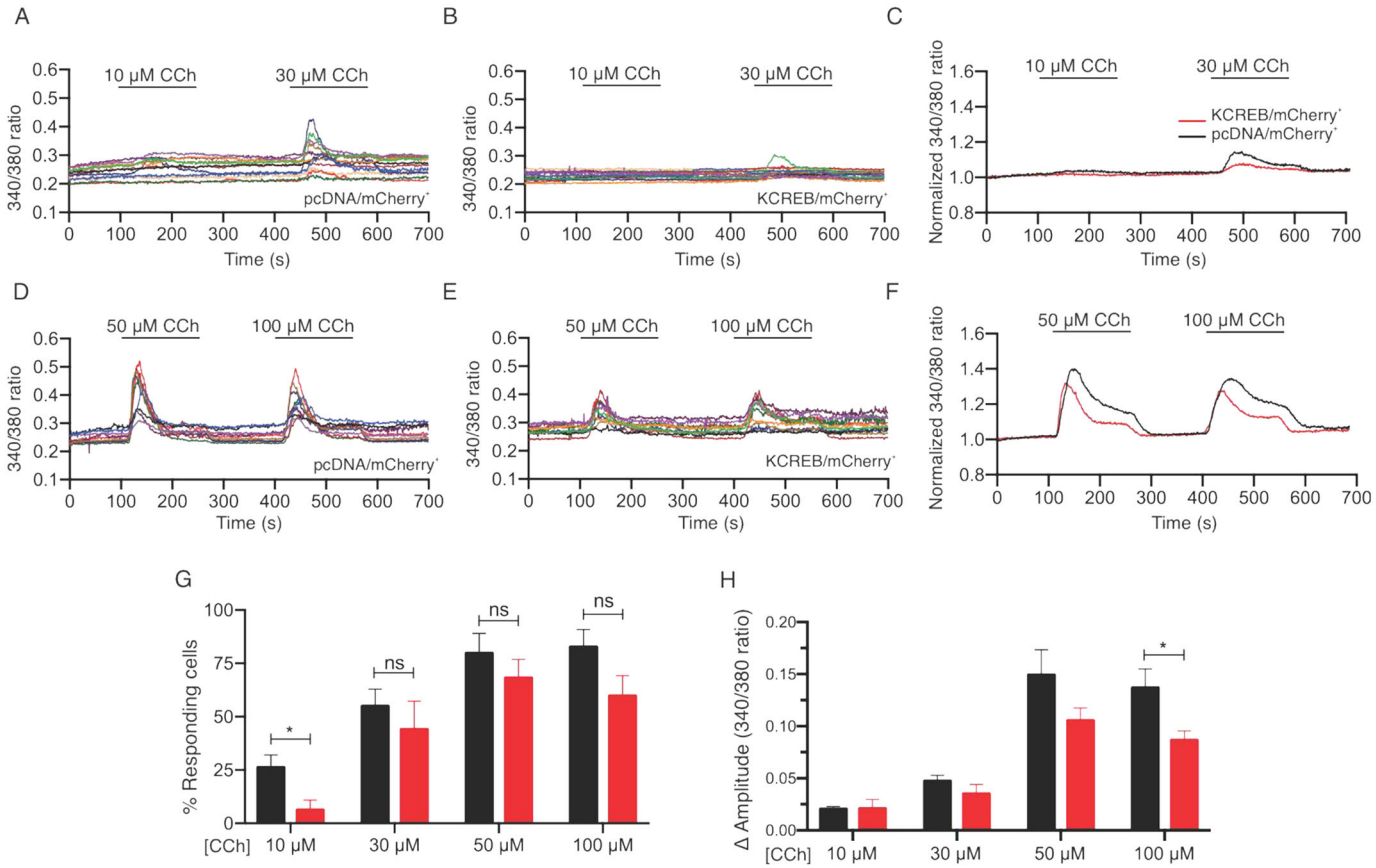

Fig. 5. Inhibition of endogenous CREB diminished CCh-induced Ca^{2+} release in single cells. hR1 endo cells transiently co-transfected with mCherry and either pcDNA or KCREB were loaded with Fura-2/AM at room temperature for 25 min followed by imaging using an inverted epifluorescence microscope. Only cells positive for mCherry were considered for analysis. (A,B,D,E) Representative Ca^{2+} traces (n=11 cells) showing increase in cytosolic Ca^{2+} from hR1 endo cells transfected with pcDNA (A,D) or KCREB (B,E) in response to CCh at 10 and 30 μM (A,B) or 50 and 100 μM (D,E). (C,F) Plotted is the average cytosolic Ca^{2+} increase in hR1 endo cells transfected with pcDNA (C: n=48 cells; F: n=62 cells) or KCREB (C: n=45 cells; F: n=50 cells) in response to CCh at 10 and 30 μM (C) or 50 and 100 μM (F). (G) Bar graph showing the percentage of responding cells (i.e. cells for which an amplitude change of >0.02 was observed), from n=7 independent experiments, in response to stimulation with CCh at 10, 30, 50 or 100 μM. Data are presented as mean±s.e.m. Statistical significance was determined by Student's t-test (unpaired, two-tailed). *P<0.05. ns, not significant. (H) Bar graph showing the change in amplitude (peak ratio – basal ratio: average of initial 20 ratio points), from n=7 independent experiments, in response to stimulation with CCh at 10, 30, 50 or 100 μM. Data are presented as mean±s.e.m. Statistical significance was determined by two-way ANOVA with Bonferroni test. *P<0.05.

HEK-293 cells augmented the endogenous levels of KRAP (Fig. 7C,D), whereas blockage of endogenous CREB by using the KCREB-expression plasmid diminished endogenous KRAP levels in HEK-293 cells (Fig. 7E,F). Moreover, endogenous KRAP levels were reduced upon transfection of the PKI-expression plasmid (Fig. 7G,H). Consistently, endogenous KRAP levels were also diminished in SH-SY5Y and HeLa cells treated with H89 (Fig. S4B,D). These results suggest a role for CREB/PKA in governing the expression of *ITPRID2* under basal and forskolin-induced conditions thus, contributing to the proper localization and appropriate activity of IP_3Rs.

In total, our results provide molecular insights to the crucial role of CREB in modulating the expression of both *ITPR1* and *ITPRID2* in HEK-293 cells. We speculate that aberrations in the levels of any of these three proteins might be an underlying cause for various pathological conditions associated with dysregulated cAMP and/or Ca^{2+} signaling.

DISCUSSION

IP_3Rs are ubiquitously expressed and, often, more than one subtype is present in any given cell type. The functional channel is assembled as a tetramer and can be homo or heterotetrameric (Foskett et al., 2007). The acute channel activity of the IP_3R is regulated by a host of regulatory factors, including IP_3, Ca^{2+}, ATP and protein-binding partners (Ferris et al., 1990; Foskett and Daniel Mak, 2010; Prole and Taylor, 2016). In addition, IP_3Rs can be phosphorylated by several kinases. In particular, an early observation was that – in response to elevated cAMP levels – IP_3Rs are phosphorylated by PKA, thereby representing a major focus of crosstalk between canonical signaling pathways (Yule et al., 2010). Although the acute effect on channel activity by regulatory factors, including those that phosphorylate PKA, has been extensively studied, there are relatively few reports of more-chronic regulatory events that have the potential to control IP_3R expression per se. For example, previous reports from our laboratory and other groups have established the roles of SP1 (Park et al., 2008, 2009), AP-1 and NFAT (Mizuno et al., 2012, 2015) in regulating *ITPR1* transcription. Similarly, the gene expression and protein synthesis of IP_3R1 are also governed by several cellular factors including TNF-α (Park et al., 2009) and TGF-β (Pacher et al., 2008; Sharma et al., 1997). However, the roles of additional factors influencing the expression of IP_3R1 remain obscure. As an important consequence of PKA activation in many cell types is to phosphorylate the transcription factor CREB – which leads to its

Journal of Cell Science (2021) 134, jcs258875. doi:10.1242/jcs.258875

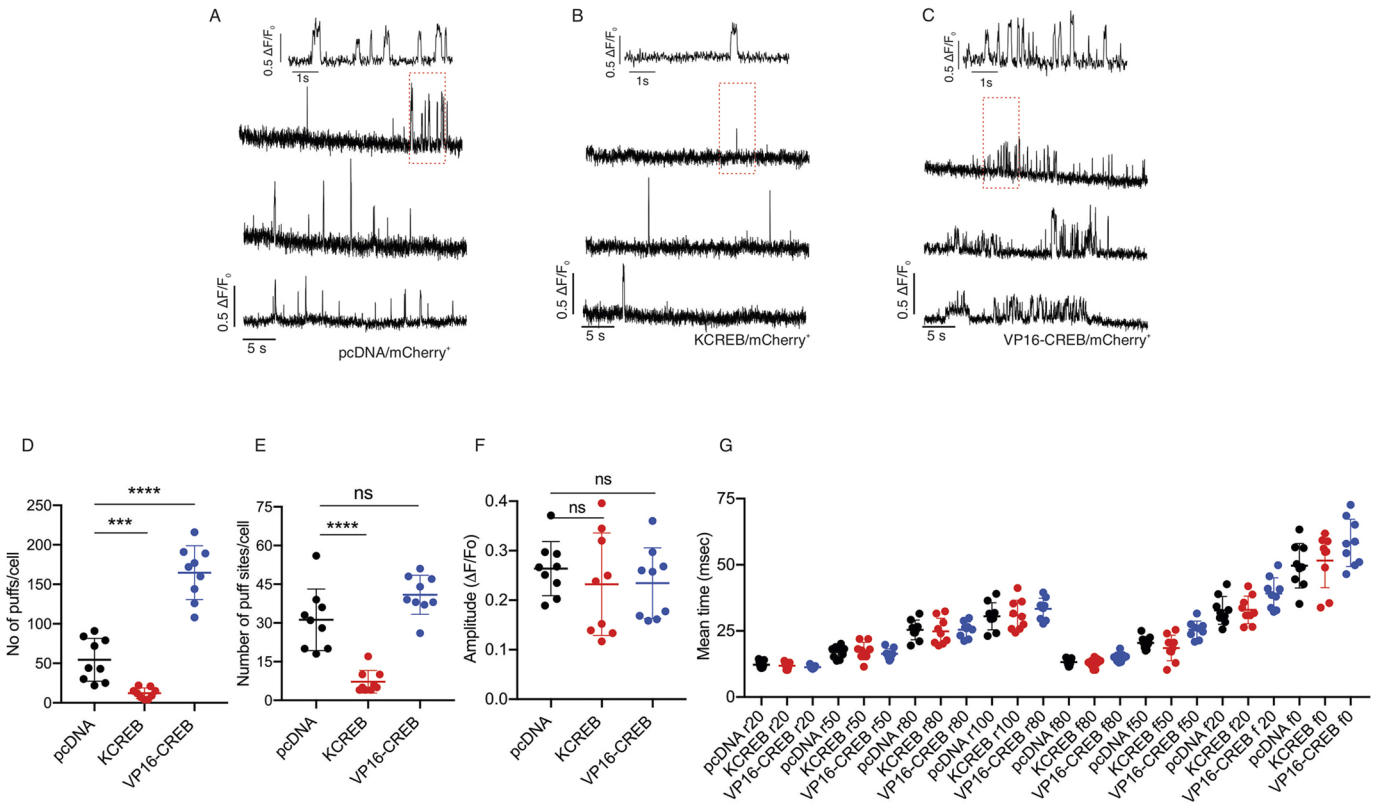

Fig. 6. CREB regulates Ca^{2+} puffs produced by IP_3R1. hR1 endo cells co-transfected with mCherry and pcDNA, VP16-CREB or KCREB plasmids (n=9 each) were loaded with Cal-520 and ci-IP_3 followed by EGTA-AM, and imaged using a TIRF microscope. A UV-flash was delivered at 3 s to uncage ci-IP_3. (A–C) Representative traces of Cal-520 fluorescence ratios ($\Delta F/F_0$) from the center of single Ca^{2+}-puff sites (1.0×1.0 µm) obtained using hR1 endo cells co-transfected with mCherry and pcDNA (A), KCREB (B) or VP16-CREB (C). Boxed regions are shown enlarged on an expanded time scale at the top of each panel. (D) The number of Ca^{2+} puffs were significantly reduced in hR1 endo cells transfected with KCREB plasmid (red) compared with those in cells transfected with pcDNA (black). In contrast, the number of Ca^{2+} puffs were significantly increased in hR1 endo cells transfected with VP16-CREB (blue) plasmid compared with those in cells transfected with pcDNA. (E) The number of Ca^{2+}-puff sites were also significantly diminished in hR1 endo cells transfected with KCREB plasmid compared with those in cells transfected with pcDNA. But the number of Ca^{2+}-puff sites were slightly higher in hR1 endo cells transfected with VP16-CREB plasmid compared with those in cells transfected with pcDNA. (F) No difference was found in the amplitude of Ca^{2+} puffs following photolysis of ci-IP_3 in hR1 endo cells transfected with pcDNA, KCREB or VP16-CREB. (G) The mean time of a 20%, 50%, 80%, or 100% rise (r) and decay (f) regarding the fluorescence of Ca^{2+} puffs evoked by photolysis of ci-IP_3 did not differ between hR1 cells transfected with pcDNA, KCREB or VP16-CREB plasmid. Only mCherry-positive cells were considered for analysis. Data are presented as mean±s.e.m. Statistical significance was determined by Student's t-test (unpaired, two-tailed). ***P<0.001, ****P<0.0001. ns, not significant.

nuclear translocation and the subsequent expression of target genes. In this current study, we investigated whether IP_3Rs are targets of transcriptional regulation by CREB and whether modulating CREB activity has any functional consequences on agonist-induced Ca^{2+} release via IP_3Rs.

We observed a significant increase in the endogenous IP_3R1 protein levels upon treatment of HEK-293 cells with 10 µM forskolin for 12 h. Protein expression of IP_3R2 and IP_3R3 subtypes in these cells, however, remained unaltered (Fig. 1). These observations are supported by evidence from the CREB target gene database, wherein the binding of CREB to the *ITPR1* promoter was augmented following treatment with forskolin for 4 h in HEK-293 T cells (binding ratio 1.7) (Zhang et al., 2005). Contrary to our observations in HEK-293 cells, a recent report provided conclusive evidence for involvement of CREB in augmenting the expression of IP_3R2 levels upon fasting or treatment of hepatocytes with forskolin (Kruglov et al., 2017). This is consistent with our observation that the reporter activities of both *ITPR1* and *ITPR2* are augmented upon overexpression of VP16-CREB in HEK-293 cells (Fig. 2). Because IP_3R2 protein levels were unaltered in HEK-293 cells, we speculate that IP_3Rs are differentially regulated by CREB, perhaps, due to differences in epigenetic modifications in a cell type-specific or tissue-specific manner.

Next, our *in silico* predictions using various tools regarding transcription factor binding revealed putative binding sites for CREB within the 1 kb proximal promoter regions of all three IP_3R subtype genes. In agreement with this, our promoter-reporter assays suggest a potential role for CREB in governing the expression of *ITPR1* and *ITPR2*. Moreover, RNAseq data mined using the GTEx portal revealed a significant positive correlation between transcript levels of *ITPR2* and *ITPR3*, and CREB across various human tissues (n=54), underscoring a potential role for CREB in regulating the gene expression of all the three IP_3R subtypes (Fig. 2). However, overexpression of CREB in HEK-293 cells resulted in a dose-dependent increase in the reporter activity and endogenous IP_3R1 protein levels, and was without any effect on the protein levels of IP_3R2 and IP_3R3 subtypes (Fig. S3). By contrast, blocking CREB resulted in a decrease in IP_3R1 levels in HEK-293 cells (Fig. 3), suggesting a key role for CREB in regulating the expression of *ITPR1* even under basal conditions. Interestingly, the *ITPR1* promoter harbors a TATA box, whereas promoters of both *ITPR2* and *ITPR3* lack a typical TATA box (Konishi et al., 1997). Initial

Journal of Cell Science (2021) 134, jcs258875. doi:10.1242/jcs.258875

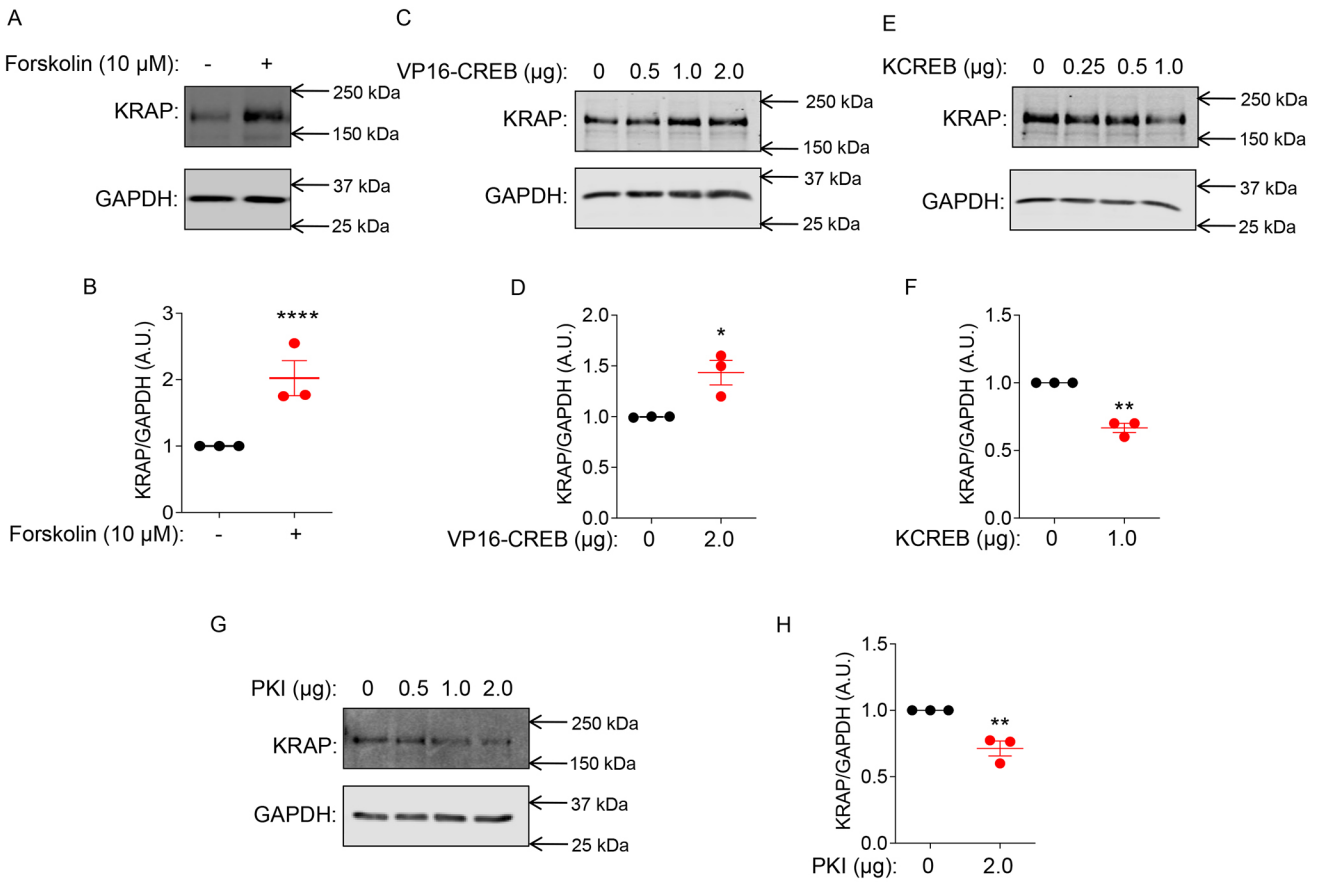

Fig. 7. CREB is crucial in governing KRAP protein levels. (A) Representative western blot showing endogenous levels of KRAP protein induced with 10 µM forskolin (+) or not induced (–) in HEK-293 cells. (B) Quantitative analysis of three independent western blots as described under A. (C,E,G) HEK-293 cells were not transfected (0), or transiently transfected with increasing amounts (0.5, 1.0, 2.0 µg) of VP16-CREB (C), increasing amounts (0.25, 0.5, 1.0 µg) of KCREB (E) or increasing amounts (0.5, 1.0, 2.0 µg) of PKI (G) expression plasmid. Total protein amounts were isolated 36 h following transfection and analyzed by western blotting. Representative western blots are shown. (D,F,H) Quantitative analysis of three independent western blots for each experimental scenario as described under C, E and G. Endogenous levels of KRAP were increased upon overexpression of VP16-CREB (C), reduced when CREB was inhibited by overexpression of KCREB (E), and reduced when PKA was inhibited by overexpression of PKI (G). Statistical significance was determined by Student's *t*-test (unpaired, two-tailed). **P*<0.05, ***P*<0.01, *****P*<0.0001.

screening showed that CREB binds to proximal TATA-box-containing promoter regions (Zhang et al., 2005); however, later investigations provided evidence that CREB can bind to distal promoter regions as well (Everett et al., 2013). This idea is further supported by the fact that *ITPR2* (which lacks a typical TATA box) can be regulated by CREB (Kruglov et al., 2017) (Fig. 2E). It is established that CREB is not recruited to promoters that are methylated (Zhang et al., 2005) and, thus, it is possible that the *ITPR2* and *ITPR3* promoters are methylated in HEK-293 cells, therefore, leading to differentially regulated gene expression of IP_3R subtypes.

CREB is a widely expressed transcription factor. During fasting, phosphorylation of CREB at Ser133 is promoted through glucagon via PKA. In turn, phosphorylated CREB augments the expression of gluconeogenic genes, including pyruvate carboxylase (PC), phosphoenolpyruvate carboxykinase 1 (PCK1) and glucose-6-phosphatase (G6PC), peroxisome proliferator-activated receptor-gamma coactivator 1 alpha (PPARGC1A) (Koo et al., 2005). Of note, glucagon also phosphorylates IP_3R1 via PKA, which results in increased cytosolic Ca^{2+} levels. This increase in cytosolic Ca^{2+} promotes CRTC2 dephosphorylation and nuclear localization of CREB-regulated transcription coactivator 2 (CRTC2), in turn, enhancing the expression of gluconeogenic genes (Wang et al., 2012). Furthermore, gluconeogenesis is promoted through glucagon via IP_3R1 in a transcriptional-independent manner (Perry et al., 2020). Strikingly, D2D transgenic mice, which are characterized by disruption of the *Itpr1* loci as well as *Itpr1* heterozygous mutant mice [also known as opisthotonos (opt/+) mice], exhibit glucose intolerance, thereby supporting a role for IP_3R1 in glucose homeostasis (Ye et al., 2011). We observed a decrease in IP_3R1 protein levels following PKI-mediated inhibition of PKA, the basal activity of which is reported to be high in HEK-293 cells (Mignen et al., 2005), as well as upon H89 treatment of SH-SY5Y and HeLa cells, both of which predominantly express the IP_3R1 subtype (Thillaiappan et al., 2021; Van Acker et al., 2002). Moreover, IP_3R1 protein levels slightly diminished in response to forskolin after blocking CREB with its dominant-negative form KCREB (Fig. 3G,H). Our results indicate that PKA, in addition to its role in phosphorylating IP_3R1, also governs the expression of IP_3R1 in various cell lines (Fig. S4A,C). This evidence suggests that Ca^{2+} release through IP_3R1 may act in a positive feedback loop via CREB to regulate *ITPR1* expression.

Does blocking the function of CREB have any effect on agonist-induced Ca^{2+} release from IP_3R1 receptors? Indeed, transient transfection of KCREB in a population-based assay revealed a modest decrease in agonist-induced Ca^{2+} release from hR1

Journal of Cell Science (2021) 134, jcs258875. doi:10.1242/jcs.258875

endo cells (Fig. 4A). However, such decrease in agonist-induced Ca^{2+} release was not observed in KCREB-transfected hR3 endo cells, reinforcing the notion that CREB does not regulate expression of *ITPR3* in HEK-293 cells (Fig. 4). We verified these results by performing single-cell imaging in hR1 endo cells transfected with the KCREB plasmid (Fig. 5).

Small but statistically significant changes were observed at lower concentration of CCh (10 µM) although no statistically significant changes were seen at higher agonist concentration. Agonist-induced Ca^{2+} release has been described within a hierarchy of Ca^{2+} release events. Ca^{2+} release from individual IP_3Rs results in blips; increased levels of IP_3 together with positive feedback through Ca^{2+}-induced Ca^{2+} release (CICR) (Foskett et al., 2007) can recruit additional IP_3Rs to generate larger events – termed Ca^{2+} puffs – that arise from a small cluster of IP_3Rs (Bootman et al., 1997; Smith and Parker, 2009; Thillaiappan et al., 2017). At greater stimulus strengths, additional IP_3R clusters are engaged through this positive feedback and Ca^{2+} signals globalize. The relatively small changes in agonist-stimulated whole-cell Ca^{2+} signals observed both in population-based and single-cell assays might be explained by the significant positive feedback due to CICR, which is measured in whole-cell assays. Additionally, at greater stimulus strengths, significant Ca^{2+} influx occurs; again, potentially, obscuring any effects of increased IP_3R levels. Notwithstanding the effects on global Ca^{2+} signals, the consequence of modulating CREB activity is – as discussed below – more significant regarding the fundamental building blocks of Ca^{2+} signals.

Research in the past decade has revealed that stimulation of all three IP_3Rs can evoke Ca^{2+} puffs of, essentially, identical properties (Lock et al., 2018; Mataragka and Taylor, 2018). Each cell type expresses several IP_3Rs, most of which are mobile and diffuse freely in the endoplasmic reticulum. In response to various stimuli or upon uncaging ci-IP_3, Ca^{2+} puffs arise repeatedly from a small fraction of localized and immobile IP_3Rs. These clusters of active IP_3Rs have been termed licensed IP_3Rs (Thillaiappan et al., 2017). KRAP associates with the N-terminal residues of IP_3Rs and co-immunoprecipitates with IP_3Rs both *in vivo* as well as in various cell lines, including HEK-293 and HeLa cells (Fujimoto et al., 2011a). Further, siRNA-mediated knockdown of KRAP diminished IP_3R-mediated Ca^{2+} release and immobilization/licensing of IP_3Rs (Fujimoto et al., 2011b; Thillaiappan et al., 2021). Thus, evidence indicates that KRAP plays a crucial role in both immobilizing IP_3R to the actin cytoskeleton and defining the activity of the licensed IP_3Rs. We, therefore, asked whether regulation of KRAP through CREB, in addition to that of IP_3R1 levels, plays a role in augmenting Ca^{2+} puff activity by, potentially, increasing the availability of this important binding partner. We observed an increase in endogenous KRAP levels upon treatment with forskolin. Similarly, the KRAP levels were regulated following overexpression of VP16-CREB, or by blocking CREB or PKA (Fig. 7 and Fig. S4B,D). In addition to regulating the expression of IP_3R1, these findings suggest that CREB/PKA activation plays a vital role in licensing of IP_3R1 through modulating the expression of KRAP. Interestingly, we observed a significant decrease in the number of Ca^{2+} puffs and Ca^{2+}-puff sites following uncaging ci-IP_3/PM upon blocking CREB in hR1 endo cells compared to control cells. This is in agreement with reduced Ca^{2+} puffs and fewer Ca^{2+}-puff sites upon siRNA-mediated knockdown of KRAP in HeLa cells (Thillaiappan et al., 2021). In contrast, the number of Ca^{2+} puffs significantly increased upon overexpression of VP16-CREB (Fig. 6), similar to those upon overexpression of KRAP in HeLa cells. We did not observe a significant increase in the number of Ca^{2+}-puff sites upon overexpression of VP16-CREB; however, the number of Ca^{2+}-puff sites significantly increased upon overexpression of KRAP in HeLa cells. These differences might be attributed to the use of different cell lines or the extent of increase in endogenous KRAP caused by overexpression of VP16-CREB (~0.5-times compared with endogenous KRAP levels in HEK-293 cells) versus overexpression of KRAP (~10-times compared with endogenous KRAP levels in HeLa cells) (Thillaiappan et al., 2021). The observed differences might also arise due to variations between HEK-293 and HeLa cells regarding the percentage of IP_3Rs and KRAP colocalizing within the TIRF field close to the plasma membrane. Nevertheless, our results underscore the functional consequences that the modulation of CREB activity, and thus IP_3R1 and KRAP, has for Ca^{2+} puffs in hR1 endo cells.

In conclusion, by using HEK-293 cells as a model cell line, our study indicates a crucial role for CREB in governing not only the expression of IP_3R1 under basal and forskolin-induced conditions but also its proper localization by regulating the levels of KRAP and, thus, the licensing of IP_3R1s destined to respond to various cues (Fig. 8). We speculate that dysregulation of CREB-mediated regulation of IP_3R1 has implications in a number of pathophysiological conditions that remain to be further investigated.

MATERIALS AND METHODS

Plasmids

VP16-CREB expression plasmid, a constitutively active form of CREB, was kindly provided by David Ginty (Harvard Medical School, Boston, MA). KCREB plasmid, a dominant-negative form of CREB, was kindly provided by Richard Goodman (Vollum Institute, Portland, OR). *ITPR2* promoter-reporter construct was kindly provided by Michael Nathanson (Yale University, New Haven, CT). pRL-TK plasmid was kindly provided by Cesare Orlandi (University of Rochester, Rochester, NY). pRSV-PKI-v2, expressing the PKA inhibitor PKI, was obtained from Addgene (#45066). pcDNA 3.1+ was from Invitrogen, USA. mCherry-3HA plasmid was generated in our laboratory. The *ITPR1* promoter-reporter construct was generated by cloning the PCR amplified 1 kb proximal promoter region of *ITPR1* (NM_001099952) between XhoI and HindIII sites in pGL3-Basic Vector (Promega, USA).

In silico predictions and GTEx data

The sequences for upstream 1 kb proximal promoter regions of *ITPR1* (NM_001099952), *ITPR2* (NM_002223), *ITPR3* (NM_002224), and *KRAP* (NM_006751) were retrieved from UCSC genome browser. Predictions for putative transcription factor-binding sites in the proximal promoter domains were performed using Alibaba2.1, TFBIND, Consite and PROMO tools. For correlation analysis between the transcript levels of *ITPRs* and CREB across various tissues, RNAseq data were mined using the GTEx portal.

Cell culture and transient transfections

HeLa, HEK-293, hR1 endo and hR3 endo cells were cultured in Dulbecco's modified Eagle's medium (DMEM) supplemented with 10% fetal bovine serum (FBS), 100 U/ml penicillin and 100 µg/ml streptomycin in 10 cm^2 cell culture dishes. SH-SY5Y cells were cultured in 1:1 mixture of Eagle's minimum essential medium (EMEM) and F12 medium supplemented with 10% FBS, 100 U/ml penicillin and 100 µg/ml streptomycin in 10 cm^2 cell culture dishes. All cell lines were obtained from ATCC. For transient transfections, cells were seeded in appropriate cell culture dishes. Following 24 h seeding, cells were transfected with indicated amounts of pcDNA, VP16-CREB, KCREB or PKI plasmids using Lipofectamine 2000 Transfection Reagent (Thermo Fisher Scientific, USA) according to the manufacturer's instructions. pcDNA was used as a balancing plasmid to transfect equal amounts of DNA in each well. Similarly, hR1 or hR3 endo cells were transfected with pcDNA or KCREB prior to imaging. In certain

Journal of Cell Science (2021) 134, jcs258875. doi:10.1242/jcs.258875

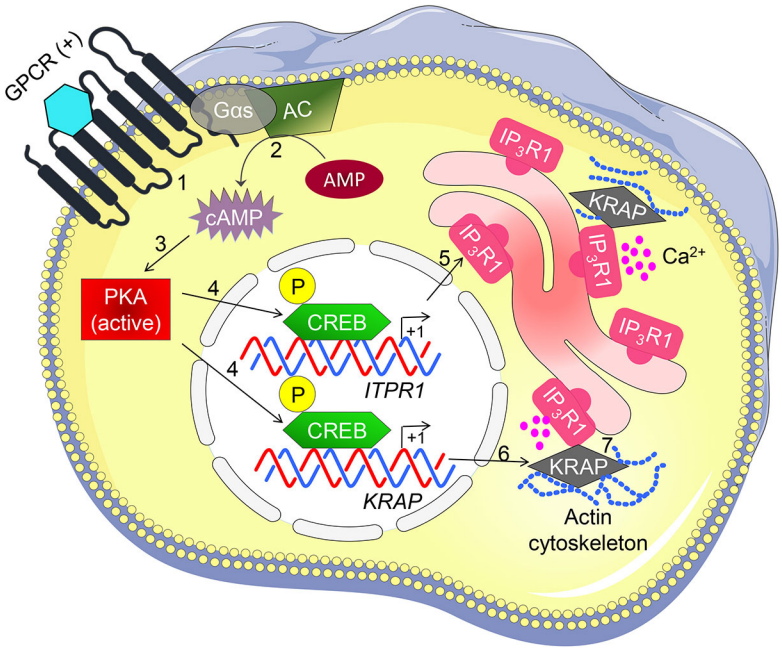

Fig. 8. Schematic depicting the involvement of the PKA–CREB axis in augmenting expression levels of IP_3R1 in HEK-293 cells. Activation of GPCR (1) augments intracellular levels of cAMP (2). cAMP promotes activation of PKA (3) that, in turn, phosphorylates CREB (4). Phosphorylated CREB enhances the endogenous protein levels of IP_3R1 (5) and KRAP (6). KRAP physically associates with IP_3R1 (7), ensuring proper localization and licensing of IP_3R1. GPCR, G protein-coupled receptor ; Gαs, G-protein alpha s subunit; AC, adenylate cyclase; AMP, adenosine monophosphate; cAMP, cyclic AMP; PKA, protein kinase A; CREB, cAMP-response element-binding protein; P, phosphorylation; IP_3R1, inositol 1,4,5-trisphosphate receptor type 1; KRAP, KRAS-induced actin-interacting protein (also known as ITPR-interacting domain containing 2, ITPRID2); (+), activated.

instances, cells were co-transfected with mCherry plasmid at a 1:10 ratio (mCherry:plasmid of interest). Cells were left in an incubator for 36 h post transfection before proceeding to western blotting or Ca^{2+} imaging.

Luciferase assays

HEK-293 cells cultured in 12-well plates were co-transfected with 250 ng of *ITPR1* or *ITPR2* promoter-reporter construct, indicated amounts of VP16-CREB or KCREB, 100 ng pRL-TK plasmid (as internal control, for normalization). pcDNA was used as a balancing plasmid to transfect equal amount of DNA in each well. Following 24–36 h transfection, cells were harvested in 1 ml PBS supplemented with 0.5 mM $MgCl_2$ and 0.1% glucose and centrifuged at 500 ***g*** for 5 min. The supernatant was discarded and cells were resuspended in 500 µl fresh PBS supplemented with 0.5 mM $MgCl_2$ and 0.1% glucose. Subsequently, 50 µl of the resuspended cells was added to each well of a white 96-well plate. To each well, 50 µl firefly luciferase substrate resuspended in lysis buffer (Promega Bright-Glo E2610) was added and incubated at room temperature in the dark for 15 min. Following 15 min incubation, luminescence was read using a plate reader. Freshly prepared Renilla buffer [1.1 M NaCl, 2.2 mM EDTA, 0.44 mg/ml BSA, 0.22 M KH_2PO_4 pH 5.1, 3 µM e-Coelenterazine (CAT#355-500, NanoLight Technology)] was added (50 µl/well), incubated at room temperature for 5 min before recording luminescence by using a plate reader. Firefly luciferase values were normalized to Renilla luciferase from respective wells and graphs are presented as percentage over control. Each experiment was performed in triplicates and repeated at least three times. To determine the effect of the PKA inhibitor H89 on *ITPR1* promoter activity, HEK-293 cells were co-transfected with 250 ng of *ITPR1* and 100 ng pRL-TK plasmid. Following 24 h transfection, cells were treated with 20 µM H89 for 12 h.

Western blotting

For western blotting, total protein was isolated from HEK-293, SH-SY5Y, HeLa control cells or cells treated with 10 µM forskolin or 20 µM H89 for 12 h using membrane-bound extraction buffer [10 mM Tris-HCl, 10 mM NaCl, 1 mM EGTA, 1 mM EDTA, 1 mMNaF, 20 mM $Na_4P_2O_7$, 2 mM Na_3VO_4, 1% Triton X-100 (v/v), 0.5% sodium deoxycholate (w/v), and 10% glycerol] supplemented with protease inhibitors. Similarly, total protein was isolated from cells transfected with pcDNA, VP16-CREB, KCREB or PKI plasmids 36 h post transfection. To determine the involvement of CREB in mediating the effects of forskolin, cells were treated with forskolin 24 h after transfection with pcDNA or KCREB and left for an additional 12 h before protein isolation. Briefly, for protein isolation, following addition of the appropriate amount of lysis buffer, cells were harvested in 1.5 ml tubes and placed on ice for 30 min. To disrupt the pellet, tubes were vortexed for 10 s every 10 min and returned on ice. Following 30 min incubation on ice, cells lysates were centrifuged at 16,000 ***g*** at 4°C for 10 min. The supernatant was transferred to newly labeled tubes. Protein concentration in the lysates was estimated using Dc protein assay kit (Bio-Rad). Lysates (30 µg) were then subjected to SDS-PAGE and transferred to a nitrocellulose membrane. Membranes were incubated with indicated primary antibodies and appropriate secondary antibodies before imaging with an Odyssey infrared imaging system (LICOR Biosciences). Band intensities were quantified using Image Studio Lite Ver 5.2 and presented as ratios of IP_3Rs/KRAP to GAPDH. The IP_3R1 antibody (#ARC154) was from Antibody Research Corporation and used at 1:1000 dilution. IP_3R2 antibody against amino acids 320–338 (NT2) was generated by Pocono Rabbit Farms and Laboratories, and used at 1:1000 dilution. IP_3R3 antibody (#610313) was from BD Transduction Laboratories and used at 1:1000 dilution. Phosphorylated IP_3 receptor (Ser1756) antibody (#3760) was from Cell Signaling Technology and used at 1:1000 dilution. Antibody for KRAP (#14157-1-AP) was from Proteintech and used at 1:1000 dilution. GAPDH (#AM4300), secondary goat anti-rabbit (SA535571) and secondary goat anti-mouse (SA535521) antibodies were from Invitrogen and used at 1:10,000 dilution.

Population-based Ca^{2+} imaging

hR1 or hR3 endo cells in 10 cm^2 cell culture dishes were transfected with 5 µg pcDNA or KCREB plasmid. Following 36 h transfection, the cells were loaded with 4 µM Fura-2/AM in cell culture medium and left in the dark for 1 hour. The cells were subsequently washed with imaging buffer (10 mM HEPES, 1.26 mM Ca^{2+}, 137 mM NaCl, 4.7 mM KCl, 5.5 mM glucose, 1 mM Na_2HPO_4, 0.56 mM $MgCl_2$, at pH 7.4). Equal numbers (300,000 cells/well) of cells transfected with pcDNA and KCREB were seeded into each well of a black-walled 96-well plate. The cells were centrifuged at 200 ***g*** for 2 min to coat the bottom of the wells and left in an incubator for another 30 min before imaging. Fura-2/AM imaging was carried out by alternately exciting loaded cells at 340 nm and 380 nm; emission was monitored at 510 nm using FlexStation 3 (Molecular Devices). Peak response to various concentrations of CCh (0.1–100 µM) was determined using SoftMax Pro Microplate Data Acquisition and Analysis software as described previously (Terry et al., 2020). Data from at least three individual plates after curve fitting using a logistic dose-response equation in GraphPad Prism 8 are presented.

Single-cell Ca^{2+} imaging

hR1 endo cells seeded on 15 mm glass coverslips in 35-mm dishes were co-transfected with mCherry plasmid (to optically identify transfected cells) and either pcDNA or KCREB. Following 36 h transfection, cells were washed with imaging buffer. Glass coverslips were attached to a Warner perfusion chamber using vacuum grease. The cells were incubated with 2 µM Fura-2/AM for 25 min in the dark at room temperature for loading. Cells were then perfused with imaging buffer and stimulated with indicated concentrations of CCh. Ca^{2+} imaging was performed using an inverted epifluorescence Nikon microscope equipped with a 40× oil immersion objective. Fura-2/AM imaging was carried out by alternately exciting loaded cells at 340 nm and 380 nm; emission was monitored at 505 nm. Images were captured every second with an exposure of 20 ms and 4×4 binning, using a digital camera driven by TILL Photonics software as previously described (Terry et al., 2020). Image acquisition was performed using TILLvisION software and data were exported to Microsoft excel. Experiments were repeated at least three times and only cells positive for mCherry were analyzed.

Detection and analysis of Ca^{2+} puffs by using TIRF microscopy

hR1 endo cells grown on 15-mm glass coverslips coated with poly-D-lysine (100 µg/ml) in a 35-mm dish for 24 h were co-transfected with 100 ng mCherry and 1 µg of pcDNA, VP16-CREB or KCREB plasmids. Following 36 h transfection and prior to imaging, cells were washed three times with imaging buffer. The cells were subsequently incubated with the Ca^{2+} dye Cal520-AM (5 µM; AAT Bioquest #21130) and caged IP3 (ci-IP_3/PM; 1 µM, Tocris #6210) in imaging buffer with 0.01% BSA in the dark at room temperature. After 1 h incubation, cells were washed three times with imaging buffer and incubated in imaging buffer containing EGTA-AM (5 µM, Invitrogen #E1219). After 45 min incubation, the medium was replaced with fresh imaging buffer and incubated for additional 30 min at room temperature to allow for de-esterification of loaded reagents.

Following loading, coverslips were mounted in a chamber and imaged using an Olympus IX81 inverted total internal reflection fluorescence microscope (TIRFM) equipped with oil-immersion PLAPO OTIRFM 60× objective lens/1.45 numerical aperture. Olympus CellSens Dimensions 2.3 (Build 189987) software was used for imaging. Cells positive for mCherry were identified by using a 561 nm laser. Subsequently, cells were illuminated by using a 488 nm laser to excite Cal-520 and emitted fluorescence was collected through a band-pass filter by a Hamamatsu ORCA-Fusion CMOS camera. The angle of the excitation beam was adjusted to achieve TIRF with a penetration depth of ∼140 nm. Images were captured from a final field of 86.7 µm×86.7 µm (400×400 pixels, one pixel=216 nm) at a rate of ∼97 frames/second (binning 2×2) by directly streaming into RAM. To photorelease IP_3, UV light from a laser was introduced to uniformly illuminate the field of view. Both the intensity of the UV flash and the duration (1 s) for uncaging IP_3 were optimized to prevent spontaneous Ca^{2+} puff activity in the absence of loaded ci-IP_3. Images were exported as vsi files. Images, 5 s before and 40 s after flash photolysis of ci-IP_3, were captured as described previously (Arige et al., 2021; Emrich et al., 2021).

The vsi files were converted to tiff files using Fiji software and further processed using FLIKA, a Python programming-based tool for image processing (Ellefsen et al., 2014). From each recording, ∼300 frames (∼3 s) were averaged before photolysis of ci-IP_3, to obtain a ratio image stack (F/F_0, with F=fluorescence, F_0=basal fluorescence) and standard deviation for each pixel for ≤30 s following photolysis. The image stack was Gaussian filtered, and pixels that exceeded the critical value of 1.0 (for our analysis) were located. The 'Detect-puffs' plug-in was used to detect the number of clusters (Ca^{2+}-puff sites), number of events (number of puffs), amplitudes and durations of localized Ca^{2+} signals from individual cells. All Ca^{2+} puffs, identified automatically by the algorithm, were manually confirmed before analysis. The results from FLIKA analysis were saved as excel files and graphs were plotted using GraphPad Prism 8.

Statistical analysis

All statistical tests were conducted using GraphPad Prism 8 and data are presented as the mean±s.e.m. Statistical significance was determined by Student's *t*-test (unpaired, two-tailed) or one-way ANOVA with Tukey's multiple comparisons post-test. *P<0.05, **P<0.01, ***P<0.001, ****P<0.0001 with respect to control condition. ns, not significant.

Acknowledgements

The authors thank David Ginty (Harvard Medical School, USA) for providing the VP16-CREB expression plasmid construct. The authors also thank Richard Goodman (Vollum Institute, USA) for providing the KCREB plasmid construct. The authors thank Michael Nathanson (Yale University, USA) for providing the *ITPR2* promoter-reporter construct. The authors thank Cesare Orlandi (University of Rochester, USA) for technical advice with luciferase assays and for providing pRL-TK plasmid. The authors thank all the members of the lab, especially Kai-Ting Huang and Amanda M. Wahl, for their valuable suggestions.

Competing interests

The authors declare no competing or financial interests.

Author contributions

Conceptualization: V.A., D.I.Y.; Methodology: V.A., L.E.T., S.M., T.R.K.; Validation: L.E.W.; Formal analysis: V.A.; Investigation: V.A., S.M.; Resources: T.R.K., L.E.W.; Data curation: V.A.; Writing - original draft: V.A.; Writing - review & editing: V.A., L.E.T., T.R.K., L.E.W., D.I.Y.; Supervision: D.I.Y.; Project administration: D.I.Y.; Funding acquisition: D.I.Y.

Funding

This work was supported by National Institutes of Health (NIH) (grant number: R01 DE014756 to D.I.Y. Deposited in PMC for release after 12 months.

Peer review history

The peer review history is available online at https://journals.biologists.com/jcs/article-lookup/doi/10.1242/jcs.258875.

References

Altarejos, J. Y. and Montminy, M. (2011). CREB and the CRTC co-activators: sensors for hormonal and metabolic signals. *Nat. Rev. Mol. Cell Biol.* **12**, 141-151. doi:10.1038/nrm3072

Alzayady, K. J. and Wojcikiewicz, R. J. H. (2005). The role of Ca2+ in triggering inositol 1,4,5-trisphosphate receptor ubiquitination. *Biochem. J.* **392**, 601-606. doi:10.1042/BJ20050949

Alzayady, K. J., Wagner, L. E., II, Chandrasekhar, R., Monteagudo, A., Godiska, R., Tall, G. G., Joseph, S. K. and Yule, D. I. (2013). Functional inositol 1,4,5-trisphosphate receptors assembled from concatenated homo- and heteromeric subunits. *J. Biol. Chem.* **288**, 29772-29784. doi:10.1074/jbc.M113.502203

Alzayady, K. J., Wang, L., Chandrasekhar, R., Wagner, L. E., II, Van Petegem, F. and Yule, D. I. (2016). Defining the stoichiometry of inositol 1,4,5-trisphosphate binding required to initiate Ca^{2+} release. *Sci. Signal.* **9**, ra35. doi:10.1126/scisignal.aad6281

Ananthanarayanan, M., Banales, J. M., Guerra, M. T., Spirli, C., Munoz-Garrido, P., Mitchell-Richards, K., Tafur, D., Saez, E. and Nathanson, M. H. (2015). Post-translational regulation of the type III inositol 1,4,5-trisphosphate receptor by miRNA-506. *J. Biol. Chem.* **290**, 184-196. doi:10.1074/jbc.M114.587030

Ando, H., Hirose, M. and Mikoshiba, K. (2018). Aberrant IP3 receptor activities revealed by comprehensive analysis of pathological mutations causing spinocerebellar ataxia 29. *Proc. Natl. Acad. Sci. USA* **115**, 12259-12264. doi:10.1073/pnas.1811129115

Arige, V., Emrich, S. M., Yoast, R. E., Trebak, M. and Yule, D. I. (2021). A protocol for detecting elemental calcium signals (Ca(2+) puffs) in mammalian cells using total internal reflection fluorescence microscopy. *STAR Protoc* **2**, 100618. doi:10.1016/j.xpro.2021.100618

Berridge, M. J. (1993). Inositol trisphosphate and calcium signalling. *Nature* **361**, 315-325. doi:10.1038/361315a0

Berridge, M. J., Lipp, P. and Bootman, M. D. (2000). The versatility and universality of calcium signalling. *Nat. Rev. Mol. Cell Biol.* **1**, 11-21. doi:10.1038/35036035

Bezprozvanny, I. (2005). The inositol 1,4,5-trisphosphate receptors. *Cell Calcium* **38**, 261-272. doi:10.1016/j.ceca.2005.06.030

Bezprozvanny, I. and Ehrlich, B. E. (1993). ATP modulates the function of inositol 1,4,5-trisphosphate-gated channels at two sites. *Neuron* **10**, 1175-1184. doi:10.1016/0896-6273(93)90065-Y

Blondel, O., Takeda, J., Janssen, H., Seino, S. and Bell, G. I. (1993). Sequence and functional characterization of a third inositol trisphosphate receptor subtype, IP3R-3, expressed in pancreatic islets, kidney, gastrointestinal tract, and other tissues. *J. Biol. Chem.* **268**, 11356-11363. doi:10.1016/S0021-9258(18)82132-9

Bootman, M. D., Berridge, M. J. and Lipp, P. (1997). Cooking with calcium: the recipes for composing global signals from elementary events. *Cell* **91**, 367-373. doi:10.1016/S0092-8674(00)80420-1

Bootman, M. D., Berridge, M. J. and Roderick, H. L. (2002). Calcium signalling: more messengers, more channels, more complexity. *Curr. Biol.* **12**, R563-R565. doi:10.1016/S0960-9822(02)01055-2

Cheung, K.-H., Mei, L., Mak, D.-O. D., Hayashi, I., Iwatsubo, T., Kang, D. E. and Foskett, J. K. (2010). Gain-of-function enhancement of IP3 receptor modal gating by familial Alzheimer's disease-linked presenilin mutants in human cells and mouse neurons. *Sci. Signal.* **3**, ra22. doi:10.1126/scisignal.2000818

Clapham, D. E. (2007). Calcium signaling. *Cell* **131**, 1047-1058. doi:10.1016/j.cell.2007.11.028

Day, R. N., Walder, J. A. and Maurer, R. A. (1989). A protein kinase inhibitor gene reduces both basal and multihormone-stimulated prolactin gene transcription. *J. Biol. Chem.* **264**, 431-436. doi:10.1016/S0021-9258(17)31276-0

De Smedt, H., Missiaen, L., Parys, J. B., Henning, R. H., Sienaert, I., Vanlingen, S., Gijsens, A., Himpens, B. and Casteels, R. (1997). Isoform diversity of the inositol trisphosphate receptor in cell types of mouse origin. *Biochem. J.* **322**, 575-583. doi:10.1042/bj3220575

Decuypere, J.-P., Monaco, G., Missiaen, L., De Smedt, H., Parys, J. B. and Bultynck, G. (2011). The IP(3) receptor-mitochondria connection in apoptosis and autophagy. *Biochim. Biophys. Acta* **1813**, 1003-1013. doi:10.4061/2011/920178

Drawnel, F. M., Wachten, D., Molkentin, J. D., Maillet, M., Aronsen, J. M., Swift, F., Sjaastad, I., Liu, N., Catalucci, D., Mikoshiba, K. et al. (2012). Mutual antagonism between IP(3)RII and miRNA-133a regulates calcium signals and cardiac hypertrophy. *J. Cell Biol.* **199**, 783-798. doi:10.1083/jcb.201111095

Ellefsen, K. L., Settle, B., Parker, I. and Smith, I. F. (2014). An algorithm for automated detection, localization and measurement of local calcium signals from camera-based imaging. *Cell Calcium* **56**, 147-156. doi:10.1016/j.ceca.2014.06.003

Emrich, S. M., Yoast, R. E., Xin, P., Arige, V., Wagner, L. E., Hempel, N., Gill, D. L., Sneyd, J., Yule, D. I. and Trebak, M. (2021). Omnitemporal choreographies of all five STIM/Orai and IP3Rs underlie the complexity of mammalian Ca(2+) signaling. *Cell Rep.* **34**, 108760. doi:10.1016/j.celrep.2021.108760

Everett, L. J., Le Lay, J., Lukovac, S., Bernstein, D., Steger, D. J., Lazar, M. A. and Kaestner, K. H. (2013). Integrative genomic analysis of CREB defines a critical role for transcription factor networks in mediating the fed/fasted switch in liver. *BMC Genomics* **14**, 337. doi:10.1186/1471-2164-14-337

Ferris, C. D., Huganir, R. L. and Snyder, S. H. (1990). Calcium flux mediated by purified inositol 1,4,5-trisphosphate receptor in reconstituted lipid vesicles is allosterically regulated by adenine nucleotides. *Proc. Natl. Acad. Sci. USA* **87**, 2147-2151. doi:10.1073/pnas.87.6.2147

Ferris, C. D., Cameron, A. M., Bredt, D. S., Huganir, R. L. and Snyder, S. H. (1991a). Inositol 1,4,5-trisphosphate receptor is phosphorylated by cyclic AMP-dependent protein kinase at serines 1755 and 1589. *Biochem. Biophys. Res. Commun.* **175**, 192-198. doi:10.1016/S0006-291X(05)81219-7

Ferris, C. D., Huganir, R. L., Bredt, D. S., Cameron, A. M. and Snyder, S. H. (1991b). Inositol trisphosphate receptor: phosphorylation by protein kinase C and calcium calmodulin-dependent protein kinases in reconstituted lipid vesicles. *Proc. Natl. Acad. Sci. USA* **88**, 2232-2235. doi:10.1073/pnas.88.6.2232

Foskett, J. K. (2010). Inositol trisphosphate receptor Ca2+ release channels in neurological diseases. *Pflugers Arch.* **460**, 481-494. doi:10.1007/s00424-010-0826-0

Foskett, J. K. and Daniel Mak, D.-O. (2010). Regulation of IP(3)R channel gating by Ca(2+) and Ca(2+) binding proteins. *Curr. Top. Membr.* **66**, 235-272. doi:10.1016/S1063-5823(10)66011-5

Foskett, J. K., White, C., Cheung, K.-H. and Mak, D.-O. D. (2007). Inositol trisphosphate receptor Ca2+ release channels. *Physiol. Rev.* **87**, 593-658. doi:10.1152/physrev.00035.2006

Fujimoto, T., Machida, T., Tanaka, Y., Tsunoda, T., Doi, K., Ota, T., Okamura, T., Kuroki, M. and Shirasawa, S. (2011a). KRAS-induced actin-interacting protein is required for the proper localization of inositol 1,4,5-trisphosphate receptor in the epithelial cells. *Biochem. Biophys. Res. Commun.* **407**, 438-443. doi:10.1016/j.bbrc.2011.03.065

Fujimoto, T., Machida, T., Tsunoda, T., Doi, K., Ota, T., Kuroki, M. and Shirasawa, S. (2011b). KRAS-induced actin-interacting protein regulates inositol 1,4,5-trisphosphate-receptor-mediated calcium release. *Biochem. Biophys. Res. Commun.* **408**, 214-217. doi:10.1016/j.bbrc.2011.03.112

Furuichi, T., Yoshikawa, S., Miyawaki, A., Wada, K., Maeda, N. and Mikoshiba, K. (1989). Primary structure and functional expression of the inositol 1,4,5-trisphosphate-binding protein P400. *Nature* **342**, 32-38. doi:10.1038/342032a0

Futatsugi, A., Nakamura, T., Yamada, M. K., Ebisui, E., Nakamura, K., Uchida, K., Kitaguchi, T., Takahashi-Iwanaga, H., Noda, T., Aruga, J. et al. (2005). IP3 receptor types 2 and 3 mediate exocrine secretion underlying energy metabolism. *Science* **309**, 2232-2234. doi:10.1126/science.1114110

Genazzani, A. A., Carafoli, E. and Guerini, D. (1999). Calcineurin controls inositol 1,4,5-trisphosphate type 1 receptor expression in neurons. *Proc. Natl. Acad. Sci. USA* **96**, 5797-5801. doi:10.1073/pnas.96.10.5797

Gerber, S., Alzayady, K. J., Burglen, L., Brémond-Gignac, D., Marchesin, V., Roche, O., Rio, M., Funalot, B., Calmon, R., Durr, A. et al. (2016). Recessive and dominant de novo ITPR1 mutations cause Gillespie syndrome. *Am. J. Hum. Genet.* **98**, 971-980. doi:10.1016/j.ajhg.2016.03.004

Graef, I. A., Mermelstein, P. G., Stankunas, K., Neilson, J. R., Deisseroth, K., Tsien, R. W. and Crabtree, G. R. (1999). L-type calcium channels and GSK-3 regulate the activity of NF-ATc4 in hippocampal neurons. *Nature* **401**, 703-708. doi:10.1038/44378

Insel, P. A. and Ostrom, R. S. (2003). Forskolin as a tool for examining adenylyl cyclase expression, regulation, and G protein signaling. *Cell. Mol. Neurobiol.* **23**, 305-314. doi:10.1023/A:1023684503883

Iwai, M., Michikawa, T., Bosanac, I., Ikura, M. and Mikoshiba, K. (2007). Molecular basis of the isoform-specific ligand-binding affinity of inositol 1,4,5-trisphosphate receptors. *J. Biol. Chem.* **282**, 12755-12764. doi:10.1074/jbc.M609833200

Joseph, S. K., Young, M. P., Alzayady, K., Yule, D. I., Ali, M., Booth, D. M. and Hajnóczky, G. (2018). Redox regulation of type-I inositol trisphosphate receptors in intact mammalian cells. *J. Biol. Chem.* **293**, 17464-17476. doi:10.1074/jbc.RA118.005624

Khan, M. T., Wagner, L., II, Yule, D. I., Bhanumathy, C. and Joseph, S. K. (2006). Akt kinase phosphorylation of inositol 1,4,5-trisphosphate receptors. *J. Biol. Chem.* **281**, 3731-3737. doi:10.1074/jbc.M509262200

Kirkwood, K. L., Homick, K., Dragon, M. B. and Bradford, P. G. (1997). Cloning and characterization of the type I inositol 1,4,5-trisphosphate receptor gene promoter. Regulation by 17beta-estradiol in osteoblasts. *J. Biol. Chem.* **272**, 22425-22431. doi:10.1074/jbc.272.36.22425

Klar, J., Hisatsune, C., Baig, S. M., Tariq, M., Johansson, A. C. V., Rasool, M., Malik, N. A., Ameur, A., Sugiura, K., Feuk, L. et al. (2014). Abolished InsP3R2 function inhibits sweat secretion in both humans and mice. *J. Clin. Invest.* **124**, 4773-4780. doi:10.1172/JCI70720

Konishi, Y., Kobayashi, Y., Kishimoto, T., Makino, Y., Miyawaki, A., Furuichi, T., Okano, H., Mikoshiba, K. and Tamura, T.-A. (1997). Demonstration of an E-box and its CNS-related binding factors for transcriptional regulation of the mouse type 1 inositol 1,4,5-trisphosphate receptor gene. *J. Neurochem.* **69**, 476-484. doi:10.1046/j.1471-4159.1997.69020476.x

Koo, S.-H., Flechner, L., Qi, L., Zhang, X., Screaton, R. A., Jeffries, S., Hedrick, S., Xu, W., Boussouar, F., Brindle, P. et al. (2005). The CREB coactivator TORC2 is a key regulator of fasting glucose metabolism. *Nature* **437**, 1109-1111. doi:10.1038/nature03967

Kruglov, E., Ananthanarayanan, M., Sousa, P., Weerachayaphorn, J., Guerra, M. T. and Nathanson, M. H. (2017). Type 2 inositol trisphosphate receptor gene expression in hepatocytes is regulated by cyclic AMP. *Biochem. Biophys. Res. Commun.* **486**, 659-664. doi:10.1016/j.bbrc.2017.03.086

Kurokawa, K., Mizuno, K. and Ohkuma, S. (2012). Possible involvement of type 1 inositol 1,4,5-trisphosphate receptors up-regulated by dopamine D1 and D2 receptors in mouse nucleus accumbens neurons in the development of methamphetamine-induced place preference. *Neuroscience* **227**, 22-29. doi:10.1016/j.neuroscience.2012.09.029

Lock, J. T., Alzayady, K. J., Yule, D. I. and Parker, I. (2018). All three IP3 receptor isoforms generate Ca(2+) puffs that display similar characteristics. *Sci. Signal.* **11**. doi:10.1126/scisignal.aau0344

Masuda, W., Betzenhauser, M. J. and Yule, D. I. (2010). InsP3R-associated cGMP kinase substrate determines inositol 1,4,5-trisphosphate receptor susceptibility to phosphoregulation by cyclic nucleotide-dependent kinases. *J. Biol. Chem.* **285**, 37927-37938. doi:10.1074/jbc.M110.168989

Mataragka, S. and Taylor, C. W. (2018). All three IP3 receptor subtypes generate Ca(2+) puffs, the universal building blocks of IP3-evoked Ca(2+) signals. *J. Cell Sci.* **131**, jcs220848. doi:10.1242/jcs.220848

Matsumoto, M., Nakagawa, T., Inoue, T., Nagata, E., Tanaka, K., Takano, H., Minowa, O., Kuno, J., Sakakibara, S., Yamada, M. et al. (1996). Ataxia and epileptic seizures in mice lacking type 1 inositol 1,4,5-trisphosphate receptor. *Nature* **379**, 168-171. doi:10.1038/379168a0

Mignen, O., Thompson, J. L. and Shuttleworth, T. J. (2005). Arachidonate-regulated Ca2+-selective (ARC) channel activity is modulated by phosphorylation and involves an A-kinase anchoring protein. *J. Physiol.* **567**, 787-798. doi:10.1113/jphysiol.2005.090209

Mignery, G. A., Südhof, T. C., Takei, K. and De Camilli, P. (1989). Putative receptor for inositol 1,4,5-trisphosphate similar to ryanodine receptor. *Nature* **342**, 192-195. doi:10.1038/342192a0

Mizuno, K., Kurokawa, K. and Ohkuma, S. (2012). Dopamine D1 receptors regulate type 1 inositol 1,4,5-trisphosphate receptor expression via both AP-1- and NFATc4-mediated transcriptional processes. *J. Neurochem.* **122**, 702-713. doi:10.1111/j.1471-4159.2012.07827.x

Mizuno, K., Kurokawa, K. and Ohkuma, S. (2015). Nicotinic acetylcholine receptors regulate type 1 inositol 1,4,5-trisphosphate receptor expression via calmodulin kinase IV activation. *J. Neurosci. Res.* **93**, 660-665. doi:10.1002/jnr.23518

Monkawa, T., Miyawaki, A., Sugiyama, T., Yoneshima, H., Yamamoto-Hino, M., Furuichi, T., Saruta, T., Hasegawa, M. and Mikoshiba, K. (1995). Heterotetrameric complex formation of inositol 1,4,5-trisphosphate receptor subunits. *J. Biol. Chem.* **270**, 14700-14704. doi:10.1074/jbc.270.24.14700

Newton, C. L., Mignery, G. A. and Südhof, T. C. (1994). Co-expression in vertebrate tissues and cell lines of multiple inositol 1,4,5-trisphosphate (InsP3) receptors with distinct affinities for InsP3. *J. Biol. Chem.* **269**, 28613-28619. doi:10.1016/S0021-9258(19)61949-6

Ogura, H., Matsumoto, M. and Mikoshiba, K. (2001). Motor discoordination in mutant mice heterozygous for the type 1 inositol 1,4,5-trisphosphate receptor. *Behav. Brain Res.* **122**, 215-219. doi:10.1016/S0166-4328(01)00187-5

Pacher, P., Sharma, K., Csordás, G., Zhu, Y. and Hajnóczky, G. (2008). Uncoupling of ER-mitochondrial calcium communication by transforming growth factor-β. *Am. J. Physiol. Renal. Physiol.* **295**, F1303-F1312. doi:10.1152/ajprenal.90343.2008

Park, K. M., Yule, D. I. and Bowers, W. J. (2008). Tumor necrosis factor-α potentiates intraneuronal Ca2+ signaling via regulation of the inositol 1,4,5-trisphosphate receptor. *J. Biol. Chem.* **283**, 33069-33079. doi:10.1074/jbc.M802209200

Park, K. M., Yule, D. I. and Bowers, W. J. (2009). Tumor necrosis factor-α-mediated regulation of the inositol 1,4,5-trisphosphate receptor promoter. *J. Biol. Chem.* **284**, 27557-27566. doi:10.1074/jbc.M109.034504

Patel, S., Joseph, S. K. and Thomas, A. P. (1999). Molecular properties of inositol 1,4,5-trisphosphate receptors. *Cell Calcium* **25**, 247-264. doi:10.1054/ceca.1999.0021

Perry, R. J., Zhang, D., Guerra, M. T., Brill, A. L., Goedeke, L., Nasiri, A. R., Rabin-Court, A., Wang, Y., Peng, L., Dufour, S. et al. (2020). Glucagon stimulates gluconeogenesis by INSP3R1-mediated hepatic lipolysis. *Nature* **579**, 279-283. doi:10.1038/s41586-020-2074-6

Prole, D. L. and Taylor, C. W. (2016). Inositol 1,4,5-trisphosphate receptors and their protein partners as signalling hubs. *J. Physiol.* **594**, 2849-2866. doi:10.1113/JP271139

Rengifo, J., Gibson, C. J., Winkler, E., Collin, T. and Ehrlich, B. E. (2007). Regulation of the inositol 1,4,5-trisphosphate receptor type I by O-GlcNAc glycosylation. *J. Neurosci.* **27**, 13813-13821. doi:10.1523/JNEUROSCI.2069-07.2007

Riccio, A., Ahn, S., Davenport, C. M., Blendy, J. A. and Ginty, D. D. (1999). Mediation by a CREB family transcription factor of NGF-dependent survival of sympathetic neurons. *Science* **286**, 2358-2361. doi:10.1126/science.286.5448.2358

Roach, J. C., Deutsch, K., Li, S., Siegel, A. F., Bekris, L. M., Einhaus, D. C., Sheridan, C. M., Glusman, G., Hood, L., Lernmark, A. et al. (2006). Genetic mapping at 3-kilobase resolution reveals inositol 1,4,5-triphosphate receptor 3 as a risk factor for type 1 diabetes in Sweden. *Am. J. Hum. Genet.* **79**, 614-627. doi:10.1086/507876

Sharma, K., Wang, L., Zhu, Y., Bokkala, S. and Joseph, S. K. (1997). Transforming growth factor-beta1 inhibits type I inositol 1,4,5-trisphosphate receptor expression and enhances its phosphorylation in mesangial cells. *J. Biol. Chem.* **272**, 14617-14623. doi:10.1074/jbc.272.23.14617

Smith, I. F. and Parker, I. (2009). Imaging the quantal substructure of single IP3R channel activity during Ca2+ puffs in intact mammalian cells. *Proc. Natl. Acad. Sci. USA* **106**, 6404-6409. doi:10.1073/pnas.0810799106

Soulsby, M. D. and Wojcikiewicz, R. J. H. (2005). The type III inositol 1,4,5-trisphosphate receptor is phosphorylated by cAMP-dependent protein kinase at three sites. *Biochem. J.* **392**, 493-497. doi:10.1042/BJ20051325

Soulsby, M. D., Alzayady, K., Xu, Q. and Wojcikiewicz, R. J. H. (2004). The contribution of serine residues 1588 and 1755 to phosphorylation of the type I inositol 1,4,5-trisphosphate receptor by PKA and PKG. *FEBS Lett.* **557**, 181-184. doi:10.1016/S0014-5793(03)01487-X

Südhof, T. C., Newton, C. L., Archer, B. T., III, Ushkaryov, Y. A. and Mignery, G. A. (1991). Structure of a novel InsP3 receptor. *EMBO J.* **10**, 3199-3206. doi:10.1002/j.1460-2075.1991.tb04882.x

Tang, T.-S., Slow, E., Lupu, V., Stavrovskaya, I. G., Sugimori, M., Llinas, R., Kristal, B. S., Hayden, M. R. and Bezprozvanny, I. (2005). Disturbed Ca2+ signaling and apoptosis of medium spiny neurons in Huntington's disease. *Proc. Natl. Acad. Sci. USA* **102**, 2602-2607. doi:10.1073/pnas.0409402102

Terry, L. E., Alzayady, K. J., Wahl, A. M., Malik, S. and Yule, D. I. (2020). Disease-associated mutations in inositol 1,4,5-trisphosphate receptor subunits impair channel function. *J. Biol. Chem.* **295**, 18160-18178. doi:10.1074/jbc.RA120.015683

Thillaiappan, N. B., Chavda, A. P., Tovey, S. C., Prole, D. L. and Taylor, C. W. (2017). Ca(2+) signals initiate at immobile IP3 receptors adjacent to ER-plasma membrane junctions. *Nat. Commun.* **8**, 1505. doi:10.1038/s41467-017-01644-8

Thillaiappan, N. B., Smith, H. A., Atakpa-Adaji, P. and Taylor, C. W. (2021). KRAP tethers IP3 receptors to actin and licenses them to evoke cytosolic Ca(2+) signals. *Nat. Commun.* **12**, 4514. doi:10.1038/s41467-021-24739-9

Tsuboi, D., Kuroda, K., Tanaka, M., Namba, T., Iizuka, Y., Taya, S., Shinoda, T., Hikita, T., Muraoka, S., Iizuka, M. et al. (2015). Disrupted-in-schizophrenia 1 regulates transport of ITPR1 mRNA for synaptic plasticity. *Nat. Neurosci.* **18**, 698-707. doi:10.1038/nn.3984

Ueasilamongkol, P., Khamphaya, T., Guerra, M. T., Rodrigues, M. A., Gomes, D. A., Kong, Y., Wei, W., Jain, D., Trampert, D. C., Ananthanarayanan, M. et al. (2020). Type 3 inositol 1,4,5-trisphosphate receptor is increased and enhances malignant properties in cholangiocarcinoma. *Hepatology* **71**, 583-599. doi:10.1002/hep.30839

Van Acker, K., Nadif Kasri, N., De Smet, P., Parys, J. B., De Smedt, H., Missiaen, L. and Callewaert, G. (2002). IP(3)-mediated Ca(2+) signals in human neuroblastoma SH-SY5Y cells with exogenous overexpression of type 3 IP(3) receptor. *Cell Calcium* **32**, 71-81. doi:10.1016/S0143-4160(02)00092-1

van de Leemput, J., Chandran, J., Knight, M. A., Holtzclaw, L. A., Scholz, S., Cookson, M. R., Houlden, H., Gwinn-Hardy, K., Fung, H.-C., Lin, X. et al. (2007). Deletion at ITPR1 underlies ataxia in mice and spinocerebellar ataxia 15 in humans. *PLoS Genet.* **3**, e108. doi:10.1371/journal.pgen.0030108

van Es, M. A., Van Vught, P. W., Blauw, H. M., Franke, L., Saris, C. G., Andersen, P. M., Van Den Bosch, L., de Jong, S. W., van 't Slot, R., Birve, A. et al. (2007). ITPR2 as a susceptibility gene in sporadic amyotrophic lateral sclerosis: a genome-wide association study. *Lancet Neurol.* **6**, 869-877. doi:10.1016/S1474-4422(07)70222-3

Wagner, L. E., II, Li, W.-H. and Yule, D. I. (2003). Phosphorylation of type-1 inositol 1,4,5-trisphosphate receptors by cyclic nucleotide-dependent protein kinases: a mutational analysis of the functionally important sites in the S2+ and S2- splice variants. *J. Biol. Chem.* **278**, 45811-45817. doi:10.1074/jbc.M306270200

Wagner, L. E., II, Li, W.-H., Joseph, S. K. and Yule, D. I. (2004). Functional consequences of phosphomimetic mutations at key cAMP-dependent protein kinase phosphorylation sites in the type 1 inositol 1,4,5-trisphosphate receptor. *J. Biol. Chem.* **279**, 46242-46252. doi:10.1074/jbc.M405849200

Wagner, L. E., II, Joseph, S. K. and Yule, D. I. (2008). Regulation of single inositol 1,4,5-trisphosphate receptor channel activity by protein kinase A phosphorylation. *J. Physiol.* **586**, 3577-3596. doi:10.1113/jphysiol.2008.152314

Walton, K. M., Rehfuss, R. P., Chrivia, J. C., Lochner, J. E. and Goodman, R. H. (1992). A dominant repressor of cyclic adenosine 3′,5′-monophosphate (cAMP)-regulated enhancer-binding protein activity inhibits the cAMP-mediated induction of the somatostatin promoter in vivo. *Mol. Endocrinol.* **6**, 647-655. doi:10.1210/mend.6.4.1350057

Wang, Y., Li, G., Goode, J., Paz, J. C., Ouyang, K., Screaton, R., Fischer, W. H., Chen, J., Tabas, I. and Montminy, M. (2012). Inositol-1,4,5-trisphosphate receptor regulates hepatic gluconeogenesis in fasting and diabetes. *Nature* **485**, 128-132. doi:10.1038/nature10988

Weerachayaphorn, J., Amaya, M. J., Spirli, C., Chansela, P., Mitchell-Richards, K. A., Ananthanarayanan, M. and Nathanson, M. H. (2015). Nuclear factor, erythroid 2-like 2 regulates expression of type 3 inositol 1,4,5-trisphosphate receptor and calcium signaling in cholangiocytes. *Gastroenterology* **149**, 211-222.e10. doi:10.1053/j.gastro.2015.03.014

Wojcikiewicz, R. J. H. (1995). Type I, II, and III inositol 1,4,5-trisphosphate receptors are unequally susceptible to down-regulation and are expressed in markedly different proportions in different cell types. *J. Biol. Chem.* **270**, 11678-11683. doi:10.1074/jbc.270.19.11678

Wojcikiewicz, R. J. H. and He, Y. Q. (1995). Type I, II and III inositol 1,4,5-trisphosphate receptor co-immunoprecipitation as evidence for the existence of heterotetrameric receptor complexes. *Biochem. Biophys. Res. Commun.* **213**, 334-341. doi:10.1006/bbrc.1995.2134

Wojcikiewicz, R. J. H. and Luo, S. G. (1998). Phosphorylation of inositol 1,4,5-trisphosphate receptors by cAMP-dependent protein kinase. Type I, II, and III receptors are differentially susceptible to phosphorylation and are phosphorylated in intact cells. *J. Biol. Chem.* **273**, 5670-5677. doi:10.1074/jbc.273.10.5670

Ye, R., Ni, M., Wang, M., Luo, S., Zhu, G., Chow, R. H. and Lee, A. S. (2011). Inositol 1,4,5-trisphosphate receptor 1 mutation perturbs glucose homeostasis and enhances susceptibility to diet-induced diabetes. *J. Endocrinol.* **210**, 209-217. doi:10.1530/JOE-11-0012

Yule, D. I., Betzenhauser, M. J. and Joseph, S. K. (2010). Linking structure to function: Recent lessons from inositol 1,4,5-trisphosphate receptor mutagenesis. *Cell Calcium* **47**, 469-479. doi:10.1016/j.ceca.2010.04.005

Zhang, X., Odom, D. T., Koo, S.-H., Conkright, M. D., Canettieri, G., Best, J., Chen, H., Jenner, R., Herbolsheimer, E., Jacobsen, E. et al. (2005). Genome-wide analysis of cAMP-response element binding protein occupancy, phosphorylation, and target gene activation in human tissues. *Proc. Natl. Acad. Sci. USA* **102**, 4459-4464. doi:10.1073/pnas.0501076102

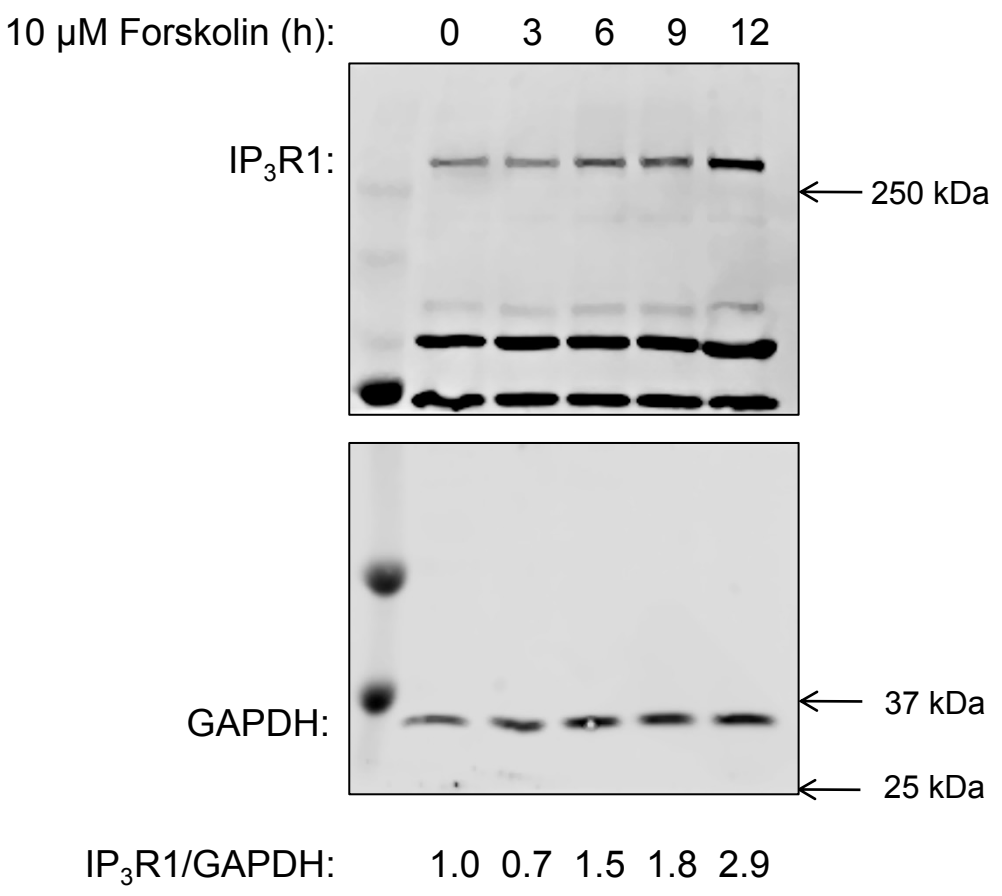

Fig. S1. Forskolin-induced endogenous IP_3R1 levels in a time-dependent manner. HEK-293 cells were treated with 10 μM forskolin for different time points (0, 3, 6, 9, 12 h). Western blotting revealed a time-dependent increase in the endogenous IP_3R1 protein levels upon forskolin treatment.

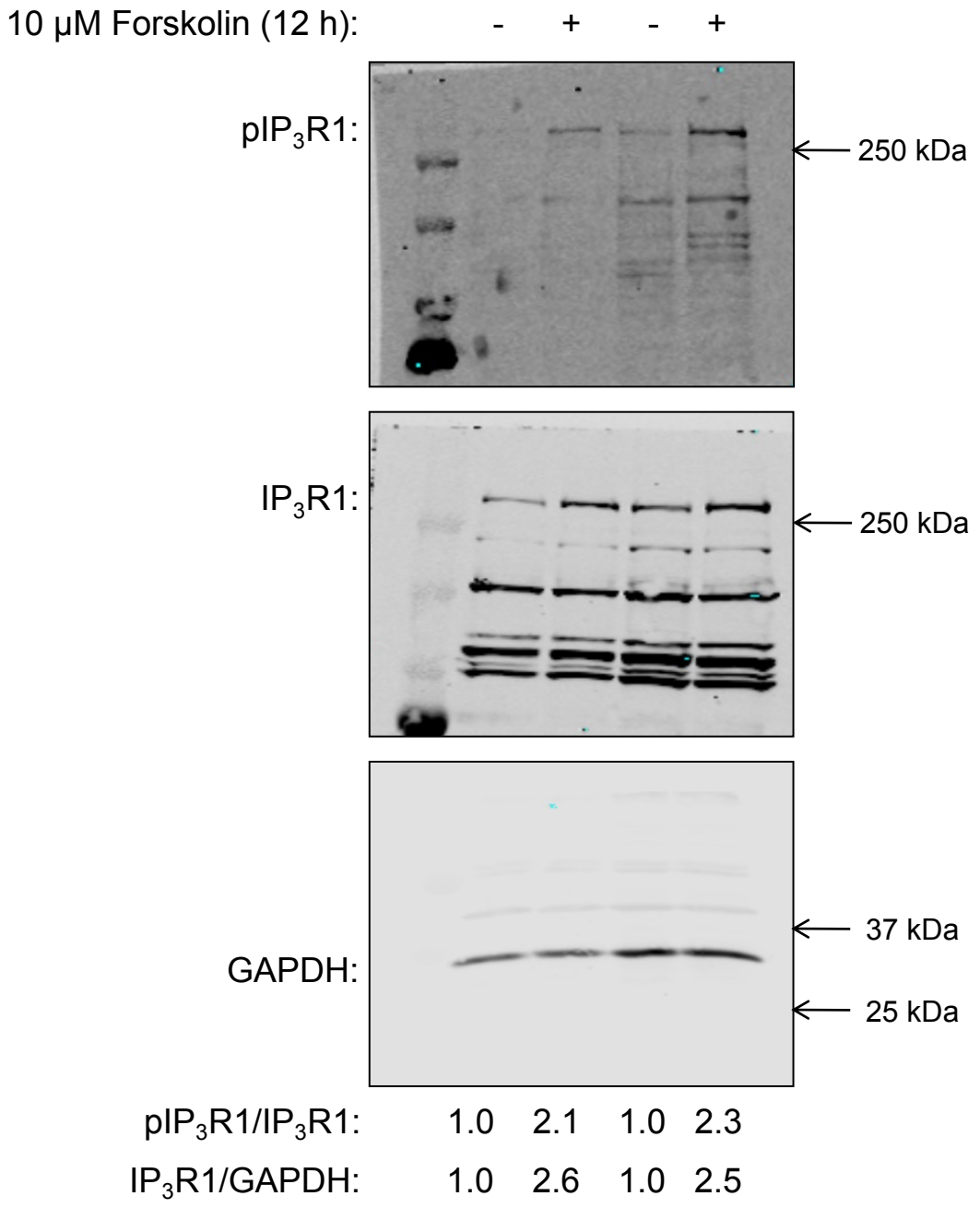

Fig. S2. Forskolin-induced phosphorylation of IP_3R1. HEK-293 cells were treated with 10 μM forskolin for 12 hours. Western blots depicting increase in the phosphorylation of the endogenous IP_3R1 at the Ser-1756 residue and total IP_3R1 protein levels upon treatment with forskolin. (Lane numbers 1 & 2: 20 μg protein and lane numbers 3 & 4: 30 μg protein was loaded).

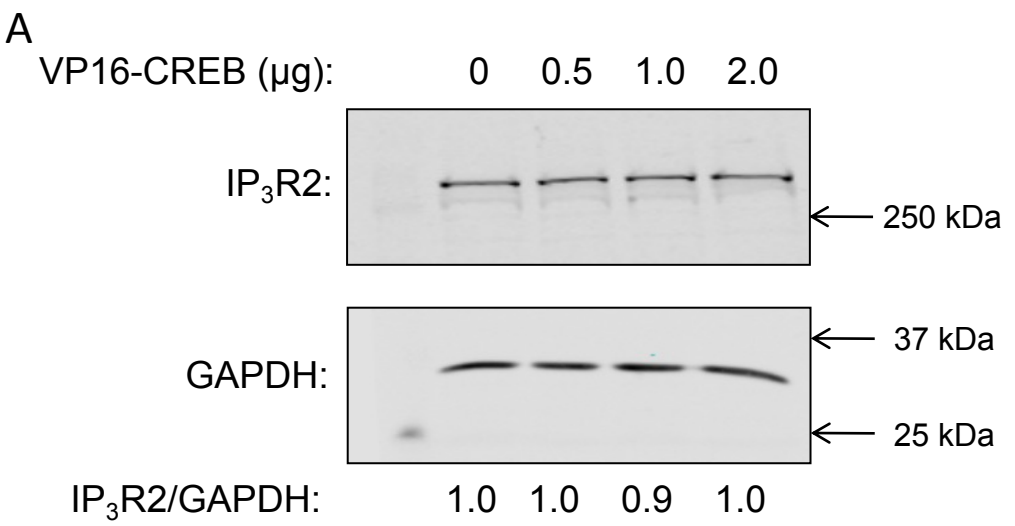

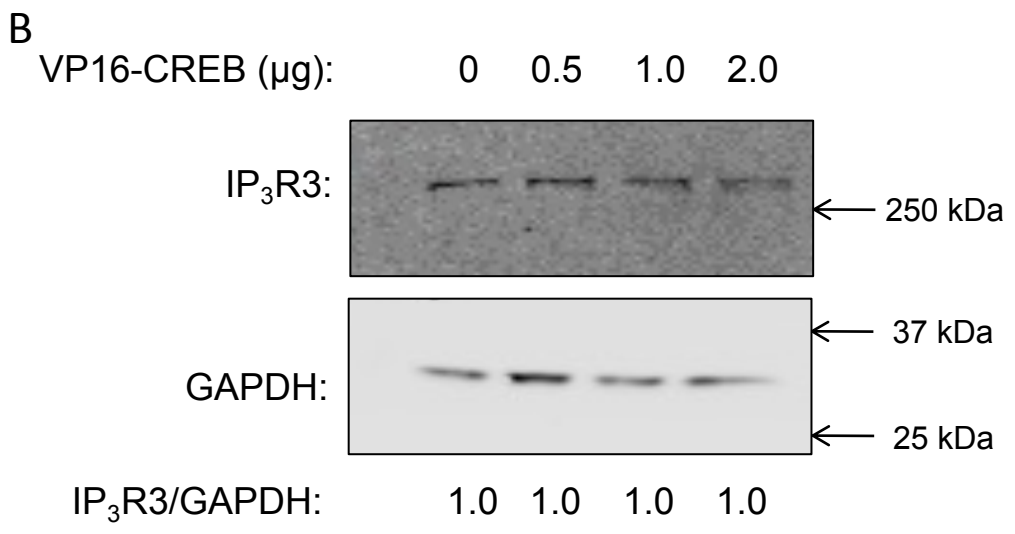

Fig. S3. CREB over-expression does not alter the endogenous protein levels of IP_3R2 and IP_3R3. HEK-293 cells were transiently transfected with increasing concentrations of VP16-CREB expression plasmid followed by Western blotting to determine the endogenous IP_3R2 and IP_3R3 protein levels using IP_3R2 and IP_3R3 specific antibodies. The endogenous (A) IP_3R2 and (B) IP_3R3 levels remained unchanged with increasing amounts of VP16-CREB expression plasmid.

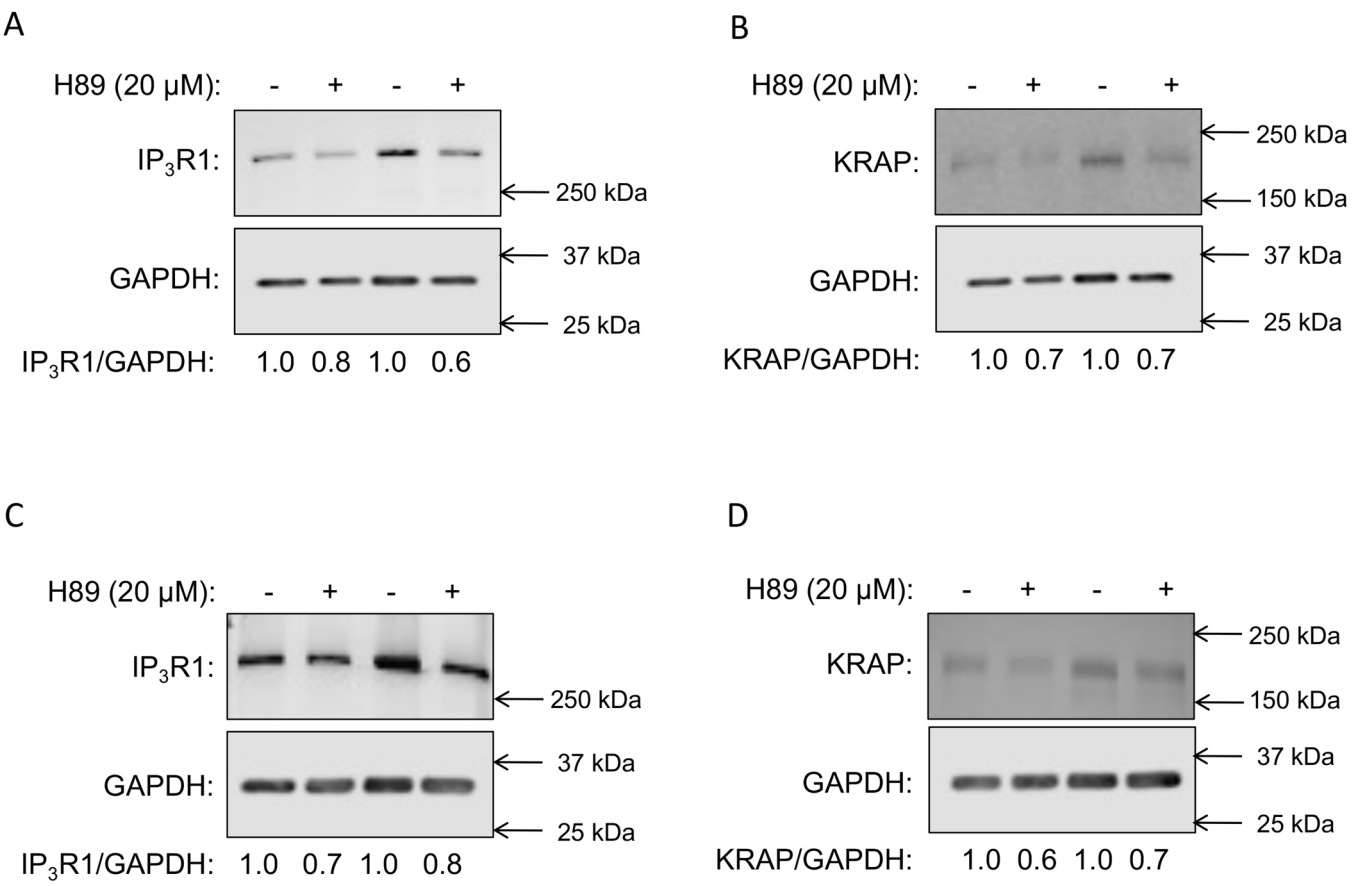

Fig. S4. H89 diminished the endogenous IP_3R1 and KRAP levels in SH-SY5Y and HeLa cells. SH-SY5Y and HeLa cells were treated with 20 μM H89 for 12 hours followed y protein isolation and Western blotting. Western blots depicting decrease in the endogenous IP_3R1 and KRAP protein levels in (A, B) SH-SY5Y and (C, D) HeLa cells upon H89 treatment. (Lane numbers 1 & 2: 20 μg protein and lane numbers 3 & 4: 30 μg protein was loaded).

Table S1. Description of the nature of tissues, number of each tissue, TPMs for $IP_3R1/2/3$ and CREB.

No.	Tissue Sample	*CREB1* (TPM)	*ITPR1* (TPM)	*ITPR2* (TPM)	*ITPR3* (TPM)
1.	Adipose – Subcutaneous (n=663)	14.61	13.4	6.854	32.57
2.	Adipose - Visceral (Omentum) (n=541)	11.72	8.267	7.814	31.19
3.	Adrenal Gland (n=258)	5.899	11.95	15.59	18.4
4.	Artery – Aorta (n=432)	14.46	52.73	6.018	9.951
5.	Artery – Coronary (n=240)	13.45	59.83	7.48	23.03
6.	Artery - Tibial (n=663)	15.68	82.02	6.701	13.03
7.	Bladder (n=21)	12.9	28.67	5.517	25.74
8.	Brain – Amygdala (n=152)	4.015	4.2	4.464	2.842
9.	Brain - Anterior cingulate cortex (n=176)	4.413	21.54	4.466	3.338
10..	Brain - Caudate (basal ganglia) (n=246)	4.189	14.34	5.018	3.643
11.	Brain - Cerebellar Hemisphere (n=215)	14.01	19.74	2.093	5.415
12.	Brain – Cerebellum (n=241)	10.66	76.19	3.348	7.016
13.	Brain – Cortex (n=255)	4.516	34.52	5.34	5.491
14.	Brain - Frontal Cortex (n=209)	5.703	38.23	4.346	3.828
15.	Brain – Hippocampus (n=197)	4.214	5.737	2.987	3.149
16.	Brain – Hypothalamus (n=202)	4.89	4.515	3.337	4.013
17.	Brain - Nucleus accumbens (n=246)	4.264	13.04	4.522	3.837
18.	Brain - Putamen (n=205)	3.518	7.7	3.582	3.324
19.	Brain - Spinal cord (n=159)	7.121	2.611	6.579	7.828
20.	Brain - Substantia nigra (n=139)	4.345	4.135	3.588	4.662
21.	Breast - Mammary Tissue (n=459)	13.35	16.03	9.494	32.45
22.	Cells - Cultured fibroblasts (n=504)	15.21	4.17	5.777	46.68
23.	Cells - EBV-transformed lymphocytes (n=174)	20.64	25.17	29.77	35.6
24.	Cervix - Ectocervix (n=9)	18.18	18.34	7.894	37.12
25.	Cervix - Endocervix (n=10)	17.36	18.44	8.11	37.35
26.	Colon – Sigmoid (n=373)	11.02	24.68	10.78	23.53

27.	Colon – Transverse (n=406)	8.59	11.21	5.755	43.48
28.	Esophagus - Gastroesophageal Junction (n=375)	9.977	40.34	5.519	24.22
29.	Esophagus – Mucosa (n=555)	9.181	5.766	10.06	31.55
30.	Esophagus - Muscularis (n=515)	9.75	41.08	6.212	22.67
31.	Fallopian Tube (n=9)	14.04	47.75	8.022	38.19
32.	Heart - Atrial Appendage (n=426)	4.623	6.396	3.523	11.35
33.	Heart - Left Ventricle (n=432)	3.437	3.212	1.535	8.767
34.	Kidney – Cortex (n=85)	3.749	7.076	4.516	12.99
35.	Kidney – Medulla (n=4)	6.812	11.92	5.666	27.96
36.	Liver (n=226)	2.865	1.304	8.559	1.829
37.	Lung (n=578)	13.63	20.26	7.498	72.36
38.	Minor Salivary Gland (n=162)	10.29	12.66	15.54	33.66
39.	Muscle – Skeletal (n=803)	3.132	1.61	1.39	3.889
40.	Nerve - Tibial (n=619)	15.74	12.7	8.456	135.8
41.	Ovary (n=180)	14.77	39.94	8.747	31.99
42.	Pancreas (n=328)	3.604	1.445	3.459	9.256
43.	Pituitary (n=283)	8.498	18.77	4.27	17.13
44.	Prostate (n=245)	11.26	20.87	5.242	33.15
45.	Skin - Not Sun Exposed (n=604)	11.32	3.817	13.62	107.1
46.	Skin - Sun Exposed (n=701)	11.21	5.94	14.71	105.5
47.	Small Intestine - Terminal Ileum (n=187)	10.8	13.55	6.769	64.36
48.	Spleen (n=241)	12.43	10.26	5.88	74.89
49.	Stomach (n=359)	6.33	6.782	4.091	36.49
50.	Testis (n=361)	17.57	6.888	3.91	44.57
51.	Thyroid (n=653)	13.48	34.69	6.175	133.3
52.	Uterus (n=142)	15.93	46..98	7.428	26.56
53.	Vagina (n=156)	13.84	12.97	8.965	56.42
54.	Whole Blood (n=755)	5.615	1.484	2.169	4.378

Table S2. *In silico* analysis revealed putative binding sites for CREB in the proximal promoter domains of KRAP gene.

Tool	Alibaba2.1	TFBIND	ConSite	PROMO
	CREB	CREB	CREB	CREB
KRAP	-	+	+	-

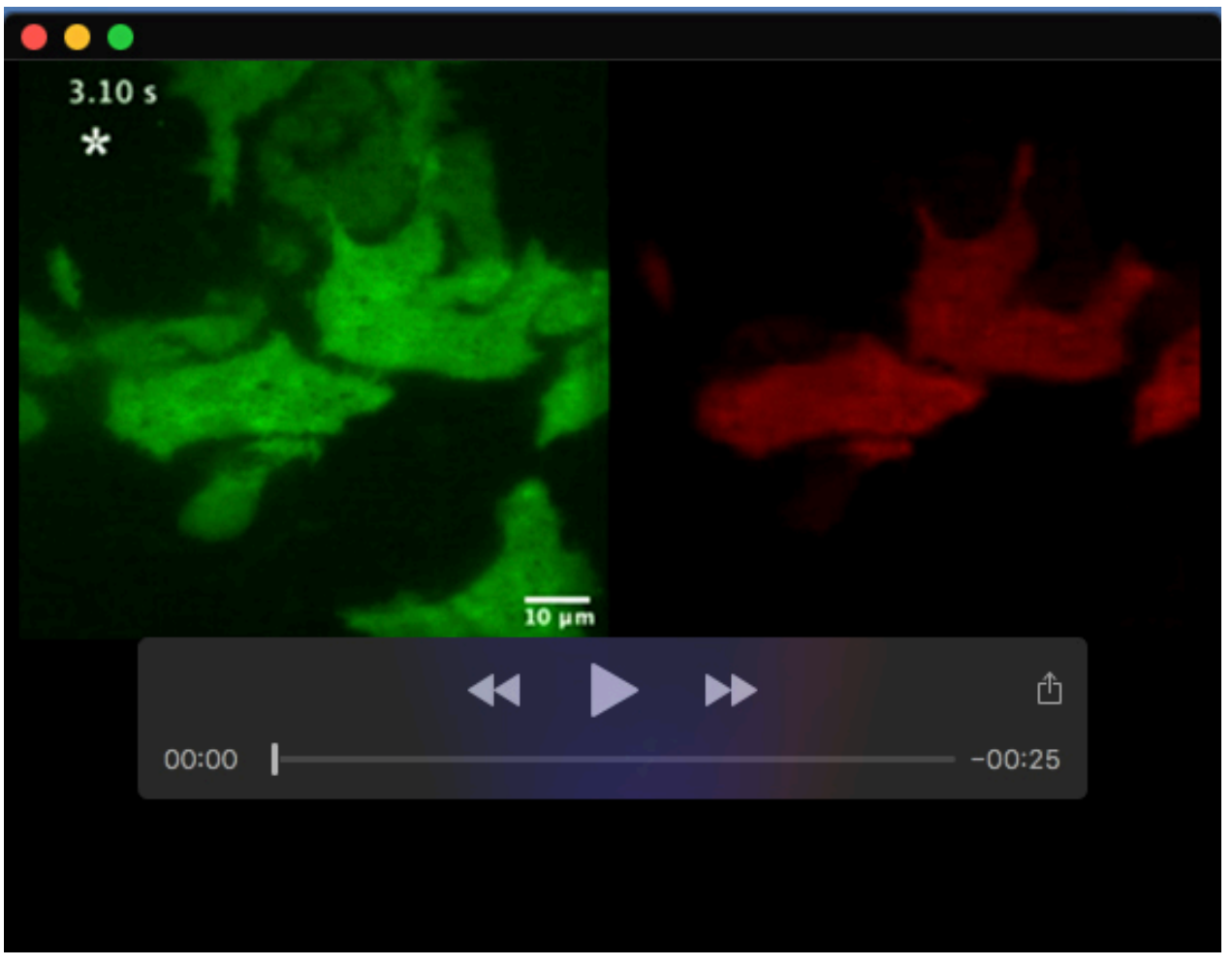

Movie 1. A typical TIRF recording from hR1 endo cells co-transfected with pcDNA and mCherry plasmid. Video showing 3 s prior to photolysis of caged ciIP_3 and the following 40 s of activity in Cal520-loaded hR1 endo cells, related to Fig. 7. Photolysis was accomplished by exposure from a 405 nm laser for 1 s (indicated by an asterisk). An image acquired from the same field of view using a 561 nm laser to optically identify mCherry positive cells is also shown.

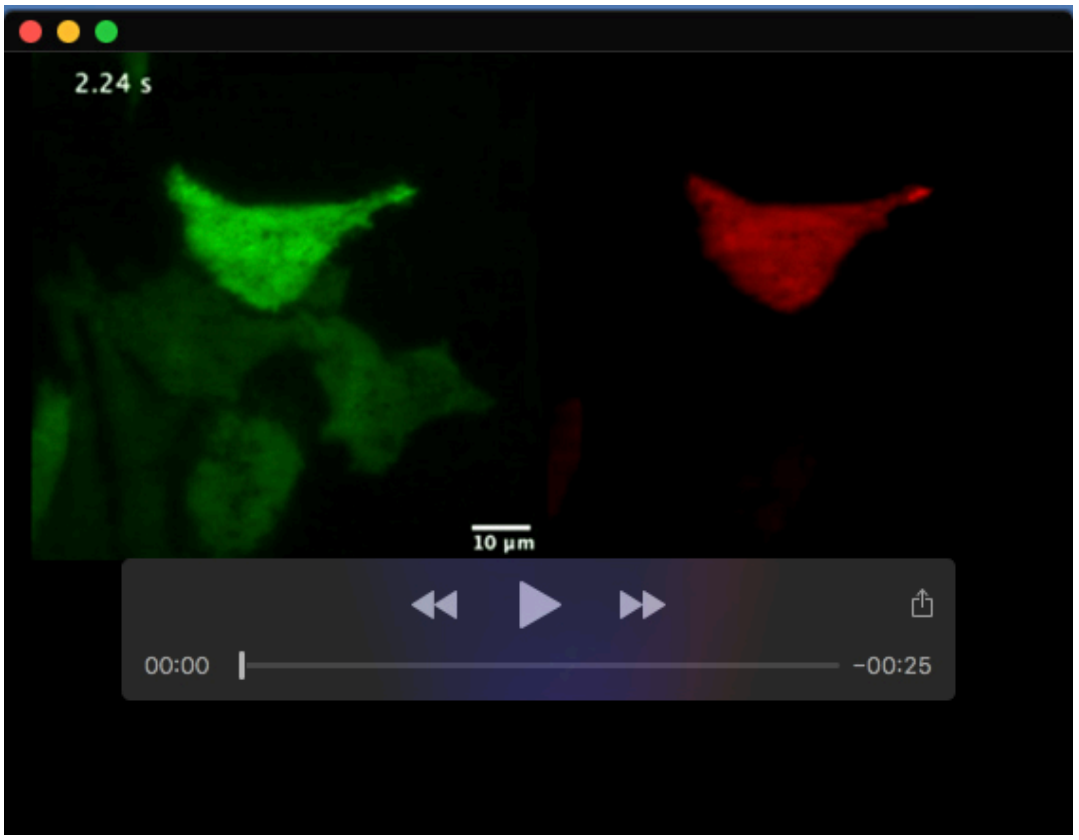

Movie 2. A typical TIRF recording from hR1 endo cells co-transfected with KCREB and mCherry plasmid. Video showing 3 s prior to photolysis of caged ciIP_3 and the following 40 s of activity in Cal520-loaded hR1 endo cells, related to Fig. 7. Photolysis was accomplished by exposure from a 405 nm laser for 1 s (indicated by an asterisk). An image acquired from the same field of view using a 561 nm laser to optically identify mCherry positive cells is also shown.

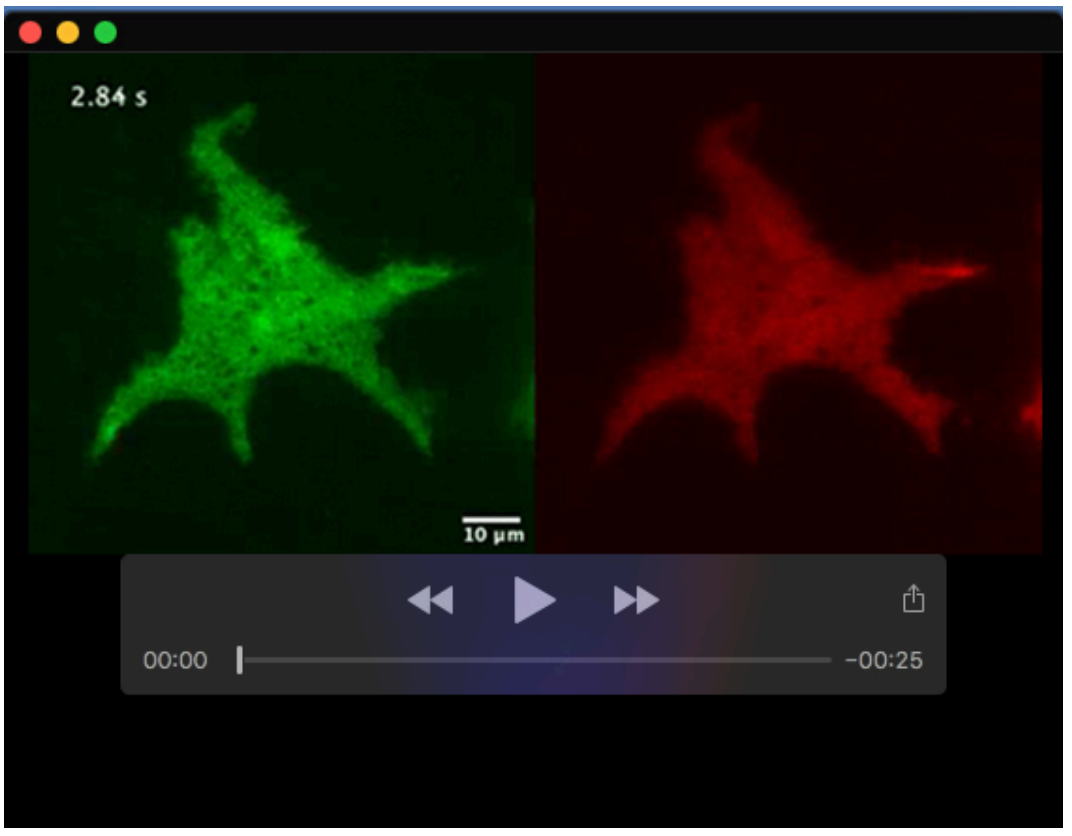

Movie 3. A typical TIRF recording from hR1 endo cells co-transfected with VP16-CREB and mCherry plasmid. Video showing 3 s prior to photolysis of caged ciIP_3 and the following 40 s of activity in Cal520-loaded hR1 endo cells, related to Fig. 7. Photolysis was accomplished by exposure from a 405 nm laser for 1 s (indicated by an asterisk). An image acquired from the same field of view using a 561 nm laser to optically identify mCherry positive cells is also shown.